

Interface collisions with diffusive mass transport

Bastien Marguet,^{1,*} F. D. A. Aarão Reis,^{2,†} and Olivier Pierre-Louis^{1,‡}

¹*Institut Lumière Matière, UMR5306 Université Lyon 1-CNRS, Université de Lyon 69622 Villeurbanne, France*

²*Instituto de Física, Universidade Federal Fluminense, Avenida Litorânea s/n, 24210-340 Niterói RJ, Brazil.*

(Dated: April 13, 2022)

We report on a linear Langevin model that describes the evolution of the roughness of two interfaces that move towards each other and are coupled by a diffusion field. This model aims at describing the closing of the gap between two two-dimensional material domains during growth, and the subsequent formation of a rough grain boundary. We assume that deposition occurs in the gap between the two domains and that the growth units diffuse and may attach to the edges of the domains. These units can also detach from edges, diffuse, and re-attach elsewhere. For slow growth, the edge roughness increases monotonously and then saturates at some equilibrium value. For fast growth, the roughness exhibits a maximum just before the collision between the two interfaces, which is followed by a minimum. The peak of the roughness can be dominated by statistical fluctuations or by edge instabilities. A phase diagram with three regimes is obtained: slow growth without peak, peak dominated by statistical fluctuations, and peak dominated by instabilities. These results reproduce the main features observed in Kinetic Monte Carlo simulations.

I. INTRODUCTION

The scenario of nucleation, growth and merging of domains is a central paradigm of non-equilibrium physics [1, 2]. However, while a very large body of work has been devoted to nucleation and to growth, little is known about merging. The collision of two interfaces that move towards each other is the elementary process that governs merging of domains. Depending on the symmetries of the order parameter that describes the domains, such a collision process might lead to the disappearance of the interfaces, as in magnetic systems similar to the Ising model, or lead to the formation of a new interface, such as a grain boundary formed by collision of two growing graphene flakes.

The existing literature on interface collisions mainly focused on domains growing side by side [3, 4]. Recently, the collision of two parallel interfaces moving towards each other and interacting only via short-range interactions has been investigated [5]. Two quantities were studied: the distribution of the collision times along the interface, and of the roughness of the newly formed interface. The asymptotic statistical properties of these two quantities were then determined exactly.

However, many interfaces exhibit long-range interactions. One major source of long-range interactions is diffusion. In this paper, we study interface collisions in diffusion-limited growth of 2D domains, with a focus on the formation of grain boundaries during the growth of 2D materials. However, beyond the study of 2D materials, we aim at developing methods for a broad class of interface collision processes that could also pertain to

diffusion-limited growth, such as solidification limited by the diffusion of temperature or by the diffusion of impurities [6, 7], and the growth of bacterial colonies limited by the diffusion of nutrients [8].

Our focus on the formation of grain boundaries in 2D materials is motivated by the relevance of the control of grain boundary roughness for applications. Indeed, several material properties such as electronic conductivity [9], thermal conductivity [10, 11] and mechanical strength [12] crucially depend on the physical properties of grain boundaries. In addition, we are also motivated by the perspective of direct comparison of our results with experiments during [13] or after [14] the collision.

Diffusion is crucial in the growth of two dimensional materials, where growth units are usually deposited between 2D domains or flakes, and then have to diffuse to the edges of the flakes where their attachment leads to growth. Since the governing laws of diffusion have no intrinsic scale, the relevant scales are those imposed by the geometry of the diffusion region, leading to long-range interactions at the scale of the diffusion region. These diffusion-limited interactions lead to several specific features.

A first well-known effect emerges from the observation that the quantity of mass deposited per unit time on the substrate between the two interfaces is proportional to the distance between them. Hence, the growth speed, which is proportional to the deposited mass, is proportional to the distance between the two interfaces. As a consequence, the interfaces slow down as they get closer to each other; this is the so-called Zeno effect [15]. As opposed to the case of non-interacting interfaces, we therefore have a time-dependent average velocity of the interfaces. Furthermore, the dependence of the growth velocity on the distance between the two edges leads to a diffusion-limited repulsion that suppresses out-of-phase edge fluctuations and leaves only in-phase fluctuations [16].

* bastien.marguet@univ-lyon1.fr

† fabioaaraoreis@gmail.com

‡ olivier.pierre-louis@univ-lyon1.fr

A second consequence of diffusion-limited dynamics is the possibility of deterministic morphological instabilities of the growing fronts. These instabilities have been studied in many systems and are referred to as the Mullins and Sekerka [17] or Bales and Zangwill [16, 18] instabilities. The roughness of the interfaces during the growth process results from a combination of these deterministic morphological instabilities and statistical fluctuations. The statistical fluctuations are known to exhibit many different regimes characterized by exponents which account for the competition between kinetic processes such as diffusion and attachment-detachment of growth units at the edge [16].

As a summary, collision of interfaces with diffusion-limited dynamics appears as a challenging problem involving time-dependent average motion of the interfaces, morphological instabilities, and kinetics-dependent statistical fluctuations. In the following, we model this process using linear Langevin equations that are derived from a Burton-Cabrera-Frank-like model [16]. Results are compared to a Kinetic Monte Carlo (KMC) model which has been reported in [19]. The Langevin model leads to features that are strikingly similar to the results of KMC simulations: (i) First, the interface roughness can exhibit a peak before or during the collision, and this peak disappears for slow growth or slow attachment-detachment kinetics. (ii) Second, the peak of roughness is followed by a sharp decrease of the roughness, and then by a slower relaxation of the newly formed interface towards equilibrium. (iii) Third, we obtain a diagram that exhibits three different regimes depending on the incoming flux and the attachment kinetics: noise-dominated peak, instability-dominated peak, and no peak.

In the following, we start with a description of the Langevin model in Section II. Then, we describe the results of the Langevin model in Section III. Finally, in Section IV, these results are compared to KMC simulations.

II. LANGEVIN MODEL

In this section, we introduce a Langevin model that aims at describing the fluctuations of the domain edges during diffusion-limited interface collisions. We start with the description of a deterministic model that accounts for deposition, diffusion, and attachment-detachment at the domain edges. Using this model, we first describe the dynamics of two straight edges moving towards each other. These fronts exhibit an exponential slowing-down when they approach each other, known as the Zeno effect [15]. Next we derive the equations that govern the evolution of perturbations of these straight edges. This analysis reveals that the edges can be stable or unstable depending on the growth conditions. Finally, we add Langevin forces that account for equilibrium and non-equilibrium statistical fluctuations.

A. Deterministic model

Some key ingredients of the model are sketched in Fig. 1. Two monolayer domains grow towards each other on a substrate. Their edges are parallel on average. The positions of the edges along the y direction are denoted as $h_{\pm}(x, t)$. We assume a constant deposition flux F of particles on the substrate between the two edges. In 2D materials such as graphene, growth units that land on top of the graphene layer often re-evaporate quickly. As a consequence, we simply neglect them, and attachment and detachment of growth units in the 2D material are considered only on the substrate side. This situation shares similarities with the Ehrlich-Schwoebel effect [20, 21] by which atoms attach preferentially from the lower side of atomic steps.

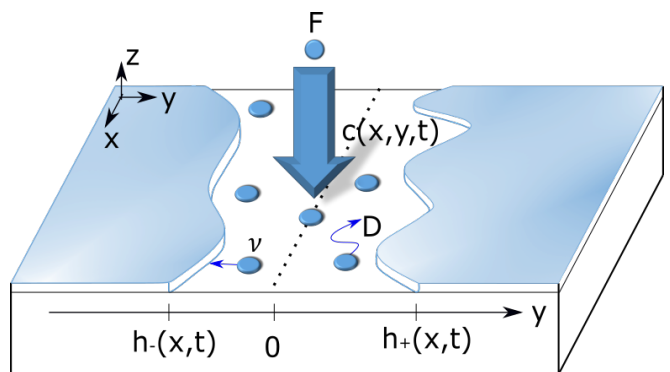


FIG. 1. Schematic: two interfaces at positions $h_+(x, t)$ and $h_-(x, t)$ grow towards each other. In the gap between the two interfaces, particles are deposited with a rate F per unit area and diffuse with a coefficient D . In addition, particles can stick to, or detach from, the edges with a kinetic coefficient ν .

The areal concentration $c(x, y, t)$ of particles obeys

$$\partial_t c(x, y, t) = D\Delta c(x, y, t) + F, \quad (1)$$

where F is the deposition rate and D is the diffusion coefficient. Assuming fast diffusion, we resort to the usual quasistatic approximation [16], where the concentration relaxes to a steady-state at a timescale which is much shorter than those related to the motion of the edges. We therefore set $\partial_t c(x, y, t) = 0$ in Eq. (1), leading to

$$0 = D\Delta c + F. \quad (2)$$

We also assume that the properties of the edges are isotropic. The normal velocity of the edges

$$v_{n\pm} = \mp \frac{\partial_t h_{\pm}(x, t)}{[1 + (\partial_x h_{\pm})^2]^{1/2}} \quad (3)$$

depends linearly on the departure from equilibrium at the edge [16]

$$\frac{v_{n\pm}}{\Omega} = \nu(c_{\pm} - c_{eq,\pm}), \quad (4)$$

where Ω is the specific area of a particle and ν is a kinetic coefficient that is dimensionally homogeneous to a velocity. Moreover, $c_{\pm} = c(x, y = \pm h(x, t), t)$ and $c_{\text{eq}, \pm}$ refer respectively to the instantaneous concentration and to the equilibrium concentration at the \pm edge. The equilibrium concentration at the edges reads [16]

$$c_{\text{eq}, \pm} = c_{\text{eq}}^0 (1 + \Gamma \kappa_{\pm}), \quad (5)$$

where κ_{\pm} is the curvature of the \pm edge. The lengthscale $\Gamma = \gamma \Omega / (k_B T)$ is proportional to the line tension of the edge γ . Finally, mass conservation at the edges reads

$$\frac{v_{n_{\pm}}}{\Omega} = \vec{n}_{\pm} \cdot (D \vec{\nabla} c_{\pm}), \quad (6)$$

where \vec{n}_{\pm} are normal vectors that point towards the substrate side by convention. The system of equations (2), (4) and (6) determines completely the dynamics of the edges.

B. Straight edges

Straight and parallel edges are a simple solution of the deterministic model. Choosing an origin of the y coordinates halfway between the two edges, we have:

$$h_{\pm}(x, t) = \pm \bar{h}^{(0)}(t). \quad (7)$$

From Eq. (2), the associated concentration field reads

$$c^{(0)}(y, t) = \bar{c}^{(0)}(t) + \frac{F}{2D} (\bar{h}^{(0)}(t)^2 - y^2), \quad (8)$$

where the concentration at the edges is obtained from Eqs. (4) and (6) as

$$\bar{c}^{(0)}(t) = c_{\text{eq}}^0 + \frac{F \bar{h}^{(0)}(t)}{\nu}. \quad (9)$$

Hence, near the edges, the concentration exceeds the equilibrium concentration by the ratio $F \bar{h}^{(0)}(t) / \nu$. This reflects the balance between deposition, which increases the concentration, and attachment, which decreases the concentration. In addition, the diffusion mass flux at the edges reads

$$\mp D \partial_y c^{(0)}(y, t) = \pm F \bar{h}^{(0)}(t). \quad (10)$$

Thus, mass conservation at the edges [Eq. (6)] leads to

$$\partial_t \bar{h}^{(0)} = -\Omega F \bar{h}^{(0)}, \quad (11)$$

$$\bar{h}^{(0)}(t) = \bar{h}^{(0)}(0) e^{-\Omega F t}. \quad (12)$$

As announced above, the two edges slow down when they approach each other. This exponential slowing-down, known as the Zeno effect [15], suggests that the two edges approach each other but never meet. The Zeno effect has been invoked as the origin of the absence of merging of mounds formed in homoepitaxial growth in the presence of a Schwoebel effect [15, 22].

C. Deterministic dynamics of perturbations around straight edges

The edge position is decomposed into the sum of its average $\pm \bar{h}^{(0)}(t)$ and of a small perturbation $h_{\pm}^{(1)}(x, t)$:

$$h_{\pm}(x, t) = \pm \bar{h}^{(0)}(t) + h_{\pm}^{(1)}(x, t), \quad (13)$$

The same decomposition is used for the concentration field

$$c(x, y, t) = c^{(0)}(y, t) + c^{(1)}(x, y, t). \quad (14)$$

In the following, we will omit the explicit dependence of h and c on the variables x, y, t unless necessary.

From (2), the perturbations of the concentration field obey

$$\partial_{xx} c^{(1)} + \partial_{yy} c^{(1)} = 0. \quad (15)$$

The linear contribution to the boundary conditions (4,6) at $y = \pm \bar{h}^{(0)}$ leads to

$$c_{\pm}^{(1)} \pm \frac{D}{\nu} \partial_y c^{(1)} \Big|_{\pm} = \pm h_{\pm}^{(1)} \left(\frac{F \bar{h}^{(0)}}{D} + \frac{F}{\nu} \right) \pm c_{\text{eq}, \pm}^0 \Gamma \partial_{xx} h_{\pm}^{(1)}. \quad (16)$$

We define the spatial Fourier transform f_q of any function $f(x)$ as

$$f_q = \int_{-\infty}^{+\infty} dx f(x) e^{-iqx}. \quad (17)$$

Performing a Fourier transform with respect to x and t , Eq.(15) is rewritten as

$$-q^2 c_q^{(1)}(y) + \partial_{yy} c_q^{(1)}(y) = 0 \quad (18)$$

and the concentration profile reads

$$c_q^{(1)}(y) = a^{(1)} \cosh(qy) + b^{(1)} \sinh(qy). \quad (19)$$

Using the boundary conditions (16) we obtain

$$a^{(1)} = \frac{\Delta h_q^{(1)}}{2U_q} \left(\frac{F \bar{h}^{(0)}}{D} + \frac{F}{\nu} - c_{\text{eq}}^0 \Gamma q^2 \right), \quad (20)$$

$$b^{(1)} = \frac{\Sigma h_q^{(1)}}{2V_q} \left(\frac{F \bar{h}^{(0)}}{D} + \frac{F}{\nu} - c_{\text{eq}}^0 \Gamma q^2 \right), \quad (21)$$

where we have defined the in-phase and out-of-phase modes of the edge perturbations

$$\Sigma h_q^{(1)} = h_{+,q}^{(1)} + h_{-,q}^{(1)}, \quad (22)$$

$$\Delta h_q^{(1)} = h_{+,q}^{(1)} - h_{-,q}^{(1)}, \quad (23)$$

and the functions of q

$$U_q = \cosh k + \frac{D}{\nu} q \sinh k, \quad (24)$$

$$V_q = \sinh k + \frac{D}{\nu} q \cosh k, \quad (25)$$

where $k = q\bar{h}^{(0)}$.

The deterministic dynamics of edge fluctuations are then obtained by substitution of Eq.(19) into mass conservation (6):

$$\partial_t \Sigma h_q^{(1)} = \lambda_{\Sigma q} \Sigma h_q^{(1)}, \quad (26)$$

$$\partial_t \Delta h_q^{(1)} = \lambda_{\Delta q} \Delta h_q^{(1)}, \quad (27)$$

where $\lambda_{\Sigma q}$ and $\lambda_{\Delta q}$ are the growth rates of the in-phase and out-of-phase modes

$$\lambda_{\Sigma q} = \frac{\Omega}{V_q} \left(F \left(k \cosh k - \sinh k \right) - D c_{\text{eq}}^0 \Gamma q^3 \cosh k \right), \quad (28)$$

$$\lambda_{\Delta q} = \frac{\Omega}{U_q} \left(F \left(k \sinh k - \cosh k \right) - D c_{\text{eq}}^0 \Gamma q^3 \sinh k \right). \quad (29)$$

A positive growth rate indicates growing perturbations, while a negative growth rate corresponds to decaying perturbations.

These growth rates include several physical effects. First, the perturbations are subject to the Mullins-Sekerka instability. Indeed, perturbations grow due to a point effect by which more atoms attach to the protuberances of the edges. This instability is decreased when attachment kinetics are slower (i.e. when ν is small). In addition, the Mullins-Sekerka instability is stronger when the incoming mass flux in the vicinity of the edges is larger. Since these mass fluxes are proportional to $\bar{h}^{(0)}$ from Eq.(10), the instability becomes weaker with time, as the average distance $2\bar{h}^{(0)}$ between the edges decreases.

Moreover, when the two edges are far from each other, perturbations from one edge are independent from those of the other edge. As the two edges approach each other, the perturbations of the two fronts become more and more coupled. One important effect of this coupling is a diffusion-limited repulsion of the two edges, leading to a strong decay of the out of phase mode. Indeed, out-of-phase perturbations lead to a spatial variation of the distance between the two edges. Since the edges slow down as they approach each other, the parts where the edges are farther from each other grow faster, while the region where the edges are closer grow slower. As a consequence, the perturbations of the out-of-phase mode decay. In contrast, this mechanism does not affect in-phase perturbations of the edges which do not lead to a spatial variation of the distance between the two edges.

Finally, line tension suppresses efficiently short wavelength perturbations of the edges. However, long-wavelength perturbations lead to a smaller increase of the total length of the edges, and thus of the total energy. Therefore, line tension does not eliminate large wavelength fluctuations as much as short wavelength modes.

Combining all these effects, the growth rates $\lambda_{\Sigma q}$ and $\lambda_{\Delta q}$ are shown on Figs. 2(a) and 2(b). We observe that an instability, which is characterized by a positive value of λ , appears for both modes. However, long-wavelength out-of-phase modes at small q are always stable, reflecting

the diffusion-limited repulsion of the two edges. In the opposite range of the spectrum, short wavelength modes at large q are always stabilized by line tension. In addition, one observes that the instability becomes weaker with time and finally disappears as $\bar{h}^{(0)}$ decreases.

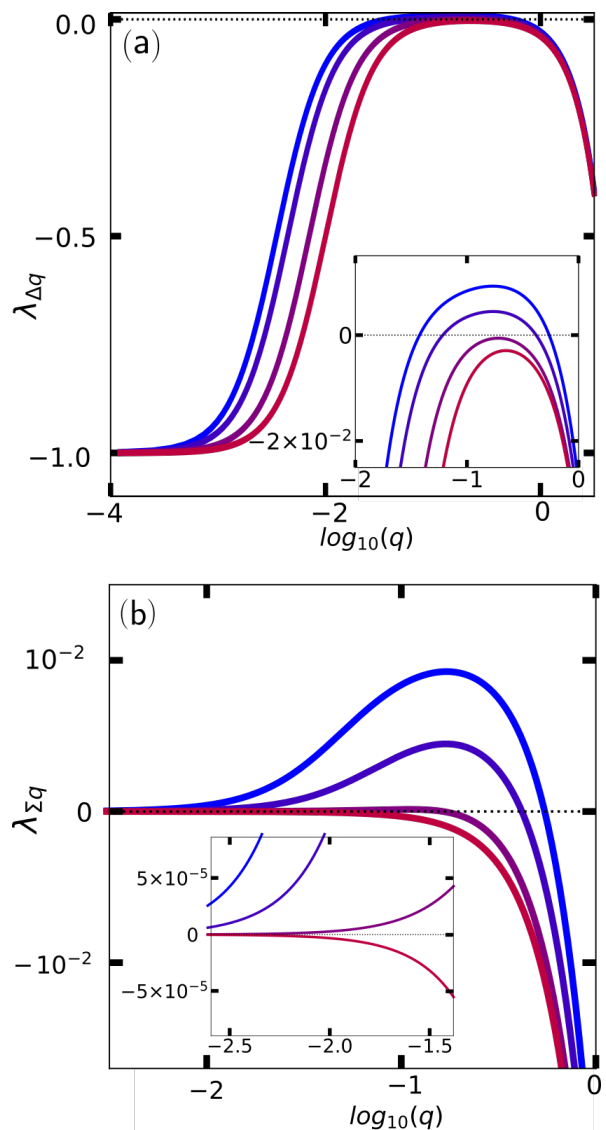


FIG. 2. Growth rate of the perturbations. (a) $\lambda_{\Sigma q}$ for the in-phase mode. (b) $\lambda_{\Delta q}$ for the out-of-phase mode. The colors correspond to different distances between the two interfaces: $\bar{h}^{(0)} = 32$ (dark blue), $\bar{h}^{(0)} = 20$ (blue), $\bar{h}^{(0)} = 8$ (violet), $\bar{h}^{(0)} = 4$ (red). An instability, corresponding to a positive $\lambda_{\Sigma q}$ or $\lambda_{\Delta q}$, is present for large $\bar{h}^{(0)}$, and disappears for small $\bar{h}^{(0)}$. We have used the following model parameters: $\Omega = 1$, $D = 10^4/4$, $c_{\text{eq}}^0 = 10^{-2}$, $\Gamma = 4.05$, $F = 1$, $\nu = 1$, $L = 512$.

D. Langevin description

The deterministic growth or decay of edge perturbations is described by Eqs. (26) and (27). Nevertheless,

these equations do not account for generation of the roughness due to statistical fluctuations. We resort to Langevin forces to describe these fluctuations:

$$\partial_t \Sigma h_q^{(1)} = \Sigma h_q^{(1)} \lambda_{\Sigma q} + \eta_{\Sigma q} + \varphi_{\Sigma q}, \quad (30)$$

$$\partial_t \Delta h_q^{(1)} = \Delta h_q^{(1)} \lambda_{\Delta q} + \eta_{\Delta q} + \varphi_{\Delta q}. \quad (31)$$

Langevin forces are separated into two contributions. The fluctuations coming from the attachment of freshly landed atoms that have not yet been attached to an edge is accounted for by the terms $\varphi_{\Sigma q}$ and $\varphi_{\Delta q}$. In contrast, the fluctuations that are related to the detachment-diffusion-reattachment of atoms lead to the contributions $\eta_{\Sigma q}$ and $\eta_{\Delta q}$. The solution of (30) and (31) reads:

$$\Sigma h_q^{(1)}(t) = \Sigma h_q^{(1)}(0) e^{\int_0^t dt' \lambda_{\Sigma q}(t')} + \int_0^t dt' \left\{ e^{\int_{t'}^t dt'' \lambda_{\Sigma q}(t'')} (\eta_{\Sigma q}(t') + \varphi_{\Sigma q}(t')) \right\}, \quad (32)$$

$$\Delta h_q^{(1)}(t) = \Delta h_q^{(1)}(0) e^{\int_0^t dt' \lambda_{\Delta q}(t')} + \int_0^t dt' \left\{ e^{\int_{t'}^t dt'' \lambda_{\Delta q}(t'')} (\eta_{\Delta q}(t') + \varphi_{\Delta q}(t')) \right\}. \quad (33)$$

The fluctuations of the each interface is characterized by its squared roughness

$$W_{\pm}^2(t) = \frac{1}{L} \int_0^L dx h_{\pm}^2 - \left(\frac{1}{L} \int_0^L dx h_{\pm} \right)^2. \quad (34)$$

However, it is more convenient to present our results using the squared roughness of the in-phase mode $\Sigma h(x, t) = h_+(x, t) + h_-(x, t)$, which is equal to two times the average $(h_+(x, t) + h_-(x, t))/2$, and of the out-of-phase mode $\Delta h(x, t) = h_+(x, t) - h_-(x, t)$, which is equal to the distance between the interfaces:

$$W_{\Sigma}^2(t) = \frac{1}{L} \int_0^L dx \Sigma h(x, t)^2 - \left(\frac{1}{L} \int_0^L dx \Sigma h(x, t) \right)^2. \quad (35)$$

$$W_{\Delta}^2(t) = \frac{1}{L} \int_0^L dx \Delta h(x, t)^2 - \left(\frac{1}{L} \int_0^L dx \Delta h(x, t) \right)^2. \quad (36)$$

The expected values of these squared roughnesses are

$$\langle W_{\Sigma}^2(t) \rangle = \frac{1}{L} \int_0^L dx \langle |\Sigma h^{(1)}|^2 \rangle = \frac{1}{L} \sum_{q \neq 0} \frac{dq}{2\pi} \langle |\Sigma h_q^{(1)}|^2 \rangle, \quad (37)$$

$$\langle W_{\Delta}^2(t) \rangle = \frac{1}{L} \int_0^L dx \langle |\Delta h^{(1)}|^2 \rangle = \frac{1}{L} \sum_{q \neq 0} \frac{dq}{2\pi} \langle |\Delta h_q^{(1)}|^2 \rangle, \quad (38)$$

where $\langle \rangle$ denotes an ensemble average over the fluctuations of the Langevin forces.

The correlations of the deposition noise φ are calculated using a simple one-dimensional model. We start from the deposition and diffusion of particles between the two edges in a discrete model, and we take the continuum limit. The details of this procedure are reported in Appendix A. Considering a periodic system of total length L along x , we find

$$\langle \varphi_{iq}(t) \varphi_{jq'}(t') \rangle = 2\Omega^2 F \bar{h}^{(0)} \delta_{i,j} \delta(t-t') \delta_{n+n'} L, \quad (39)$$

where the indices i and j indicate either Σ or Δ . In addition, the index n accounts for Fourier modes along x with wavenumber $q = 2\pi n/L$.

As opposed to the deposition process, which is an unbalanced irreversible process in our model, the detachment-diffusion-reattachment of atoms can be balanced in such a way to obtain a well-defined equilibrium. We therefore resort to a different approach based on the fluctuation-dissipation theorem to calculate the correlations of η [23]. Since this process is independent from that of the diffusion of freshly landed atoms, we consider an equilibrium state by simply setting $F = 0$. We then obtain from (30) and (31)

$$\partial_t \Sigma h_q^{(1)} = -\Sigma h_q^{(1)} \Omega D c_{\text{eq}}^0 \Gamma q^3 \frac{\cosh k}{V_q} + \eta_{\Sigma q}, \quad (40)$$

$$\partial_t \Delta h_q^{(1)} = -\Delta h_q^{(1)} \Omega D c_{\text{eq}}^0 \Gamma q^3 \frac{\sinh k}{U_q} + \eta_{\Delta q}. \quad (41)$$

Since equilibrium is a stationary process in time and the system properties are spatially homogeneous along x , fluctuations are a stationary process along time t and space x . We therefore assume that the autocorrelation of η takes the form

$$\langle \eta_{\Sigma q}(t) \eta_{\Sigma q'}(t') \rangle = \delta_{n+n'} \delta(t-t') B_{\Sigma q} L, \quad (42)$$

$$\langle \eta_{\Delta q}(t) \eta_{\Delta q'}(t') \rangle = \delta_{n+n'} \delta(t-t') B_{\Delta q} L. \quad (43)$$

where $B_{\Sigma q}$ and $B_{\Delta q}$ are constants. As a consequence, the roughness of the edges depends on $B_{\Sigma q}$ and $B_{\Delta q}$ in our model. However, in equilibrium, the static spectrum is completely determined by the line stiffness $\tilde{\gamma}$ of the edge [16]:

$$\langle |h_q^{(1)}|^2 \rangle_{\text{eq}} = \frac{k_B T}{\tilde{\gamma} q^2} L. \quad (44)$$

The roughness therefore reads:

$$\langle |W^2| \rangle_{\text{eq}} = \frac{1}{L^2} \sum_{n \neq 0} \langle |h_q^{(1)}|^2 \rangle_{\text{eq}} = \frac{k_B T L}{12 \tilde{\gamma}} = \frac{\Omega L}{12 \Gamma}. \quad (45)$$

The consistency of this equilibrium expression with the expression of the roughness as a function of $B_{\Sigma q}$ and $B_{\Delta q}$ imposes the expression of the two amplitudes

$$B_{\Sigma q} = 4\Omega^2 D c_{\text{eq}}^0 \left[\frac{q \cosh k}{V_q} \right], \quad (46)$$

$$B_{\Delta q} = 4\Omega^2 D c_{\text{eq}}^0 \left[\frac{q \sinh k}{U_q} \right]. \quad (47)$$

Since the correlations of the noise are now completely determined, we obtain the expression of the two contributions to the time-dependent roughness from the combination of Eqs.(32,37,38)

$$\langle W_{\Sigma}^2 \rangle = \frac{1}{L^2} \sum_{n \neq 0} \{ |\Sigma h_q^{(1)}(0)|^2 e^{2 \int_0^t dt' \lambda_{\Sigma q}} + L \int_0^t dt' \{ e^{2 \int_0^{t'} dt'' \lambda_{\Sigma q}} (B_{\Sigma q} + 2\Omega^2 F \bar{h}^{(0)}) \} \}, \quad (48)$$

$$\langle W_{\Delta}^2 \rangle = \frac{1}{L^2} \sum_{n \neq 0} \{ |\Delta h_q^{(1)}(0)|^2 e^{2 \int_0^t dt' \lambda_{\Delta q}} + L \int_0^t dt' \{ e^{2 \int_0^{t'} dt'' \lambda_{\Delta q}} (B_{\Delta q} + 2\Omega^2 F \bar{h}^{(0)}) \} \}. \quad (49)$$

To evaluate these expressions numerically, we integrate their time-derivative instead of calculating directly the integrals over time. We therefore evaluate the power spectral density $\langle |\Sigma h_q^{(1)}(t)|^2 \rangle$ of the Σ contribution to the roughness for each mode q by solving

$$\partial_t \langle |\Sigma h_q^{(1)}(t)|^2 \rangle = 2\lambda_{\Sigma q}(t) \langle |\Sigma h_q^{(1)}(t)|^2 \rangle + B_{\Sigma q} L + 2\Omega^2 F \bar{h}^{(0)} L \quad (50)$$

with an Euler scheme. A similar procedure is used for the Δ contribution to the roughness.

III. RESULTS OF THE LANGEVIN MODEL

A. Temporal evolution of the roughness

We have investigated the dynamics starting from straight edges at $t = 0$, i.e. for all q

$$\langle |\Sigma h_q^{(1)}(0)|^2 \rangle = \langle |\Delta h_q^{(1)}(0)|^2 \rangle = 0. \quad (51)$$

Different types of evolution appear depending on the incoming flux F . They are reported in Fig. 3.

For small fluxes, the in-phase and out-of-phase roughnesses are initially identical and grow due to statistical fluctuations. Then, when the two interfaces get closer to each other, the out-of-phase roughness decreases quickly due to the diffusive repulsion between the two interfaces. However, the in-phase roughness still grows and then reaches a constant asymptotic value.

When the incoming flux is increased, the roughness exhibits a faster increase at short times. Once again, the out-of-phase roughness decreases quickly when the two interfaces approach each other. However, the in-phase roughness also decreases when the interfaces get closer to each other. Finally, at long times, the in-phase roughness starts to increase again and reaches the same asymptotic value, which does not depend on the flux.

In the following sections, we discuss the features of the temporal evolution of the roughnesses in more details.

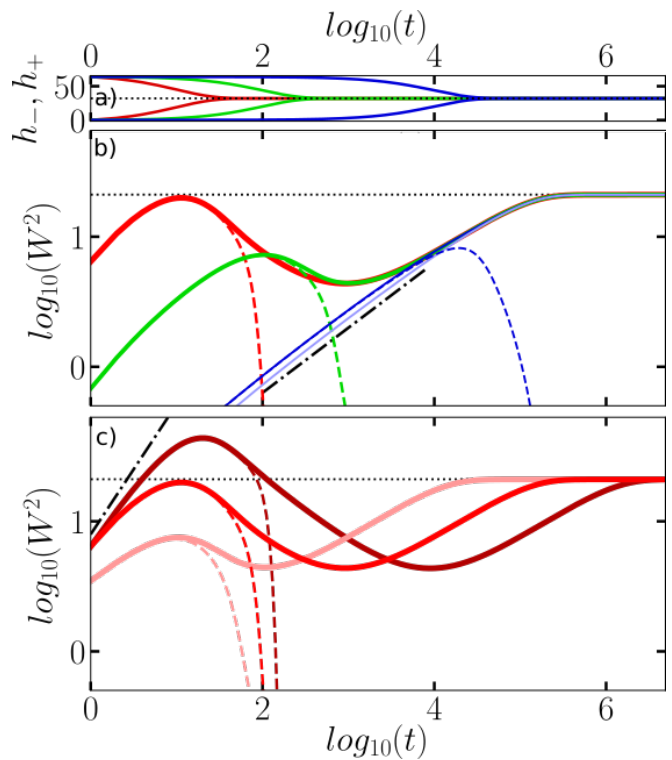


FIG. 3. Average closing of the gap and evolution of the roughness. a) Evolution of the interfaces average position. b) Roughness of the in-phase mode (solid curves) and out-of-phase mode (dashed curves) for $\nu = 1$ and different fluxes: $F = 10^{-1}$ (red), $F = 10^{-2}$ (green), and $F = 10^{-4}$ (blue). c) Roughness of the in-phase and out-of-phase modes for $F = 10^{-1}$ and different kinetic coefficients: $\nu = 10^{-1}$ (dark red), $\nu = 1$ (red), and $\nu = 10^1$ (light red). Other model parameters: $\Omega = 1$, $D = 10^4/4$, $c_{\text{eq}}^0 = 10^{-2}$, $\Gamma = 4.05$, $L = 512$, and $\bar{h}^{(0)}(0) = 32$. The horizontal black dotted line represents W_{eq}^2 , the squared equilibrium roughness. The dash-dotted black lines indicate the slopes associated to power-law behaviors: $W_{\Sigma}^2 \propto t^{1/2}$ in (b) and $W_{\Sigma}^2 \propto t$ in (c).

B. Short-time Random-Deposition roughening

An expansion of Eq.(48) with flat initial conditions (51) shows that the squared roughness is linear in time at short times:

$$\langle W_{\Sigma}^2 \rangle = \left(\Omega c_{\text{eq}}^0 \chi + \Omega F \frac{h^{(0)}(0)}{a} \right) 2\Omega t, \quad (52)$$

where a is a microscopic cutoff along x . The total number of modes is set to $L/2a$, which implies a cut-off for the smallest wavelength $\lambda_c = 2a$. In addition, we have defined the kinetic factor χ , which obeys $\chi = \pi D/a^2$ for fast attachment kinetics $\nu/Dh^{(0)}(0) \gg 1$ and $\chi = 2\nu/a$ for slow attachment kinetics $\nu/Dh^{(0)}(0) \ll 1$. The derivation of Eq.(52) is provided in Appendix C. This linear behavior is also found in the full numerical solution of the Langevin model, as seen in Fig. 4. Other examples of this regime are reported in Fig. 15 of Appendix C.

Such a linear behavior of the square roughness is associated to the Random Deposition (RD) process, where uncorrelated attachment or detachment events start to roughen the interface at short times [16, 24].

While the first term in Eq.(52) accounts for the equilibrium detachment or detachment-diffusion-reattachment events, the second term accounts for deposition-diffusion-attachment events. Note also that $\langle W_\Sigma^2 \rangle$ at short times depends on the microscopic cutoff a along the x axis.

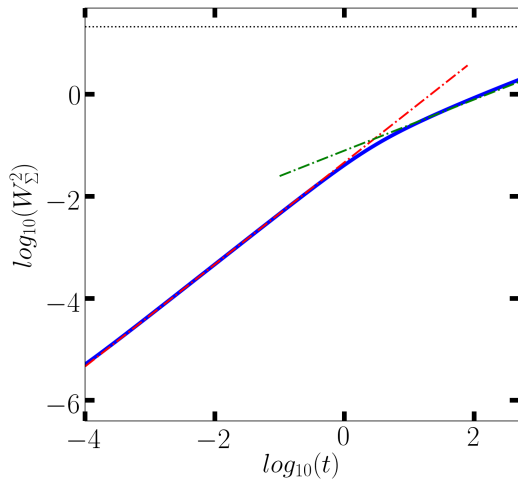


FIG. 4. Short-time behavior of the roughness of the in-phase mode (blue curve). Red dash-dotted line: asymptotic behavior $W_\Sigma^2 \propto t$ from Eq. (52). Green dash-dotted line: asymptotic behavior $W_\Sigma^2 \propto t^{1/2}$ from Eq. (57). The other model parameters are: $\Omega = 1$, $D = 10^4/4$, $c_{\text{eq}}^0 = 10^{-2}$, $\Gamma = 4.05$, $L = 512$, $\bar{h}^{(0)}(0) = 32$, $\nu = 1$, and $F = 10^{-4}$.

C. Asymptotic equilibrium roughness

In the opposite limit of long times, the in-phase roughness reaches a constant value, while the out-of-phase modes are efficiently eliminated by the diffusive repulsion between the two interfaces, so that $\langle W_\Delta^2 \rangle \rightarrow 0$. Since the amplitude of the out-of-phase modes vanishes, the interface is composed of the two in-phase edges, which have identical profiles at long times. As a consequence, this effective interface with the two edges exhibits fluctuations that are identical to that of an interface at equilibrium with a line stiffness $2\tilde{\gamma}$. The profile of the effective interface is $(h_+ + h_-)/2 = \Sigma h/2$, and as a consequence its roughness is $\langle W_\Sigma^2 \rangle/4$. Using the equilibrium formula [Eq.(45)] for the effective interface with doubled line tension, we obtain $\langle W_\Sigma^2 \rangle/4 = \Omega L/(12 \times 2\Gamma)$. This leads to the asymptotic roughnesses

$$\langle W_\Sigma^2 \rangle = \frac{\Omega L}{6\Gamma}, \quad (53)$$

$$\langle W_\Delta^2 \rangle \rightarrow 0. \quad (54)$$

As seen in Fig. 3, this result is in quantitative agreement with the asymptotic value of $\langle W_\Sigma^2 \rangle$ in the full numerical

solution of the Langevin model.

D. Close to equilibrium Edwards-Wilkinson roughening

In the limit of small fluxes F [blue curve in Fig 3(b)], the roughness slowly builds up and increases monotonically up to its equilibrium value (53). Since the power-spectrum at equilibrium (44) is dominated by long wavelengths, i.e. small q , we expect that a long-wavelength expansion can catch the main features of the convergence towards equilibrium. In the limit $q \rightarrow 0$, a relatively simple expression of $\langle W_\Sigma^2 \rangle$ can be obtained

$$\langle W_\Sigma^2 \rangle = \frac{\Omega L}{2\pi^2\Gamma} \sum_{n \neq 0} \frac{1}{n^2} (1 - e^{-vn^2}), \quad (55)$$

where

$$v = 2\Omega\Gamma \left(\frac{2\pi}{L} \right)^2 \frac{\nu c_{\text{eq}}^0}{\Omega F} \ln \frac{1 + \frac{D}{\nu \bar{h}^{(0)}(t)}}{1 + \frac{D}{\nu \bar{h}^{(0)}(0)}} > 0. \quad (56)$$

The derivation of this relation, reported in Appendix B, relies on the assumption that $\lambda_{\Sigma q}$ and the noise in Eq.(50) can be approximated by their values at zero flux. The effect of the flux is then only to drive the average motion of the edges.

From Eq.(55), we find that the roughness tends to the equilibrium value of Eq.(53) at long times. Indeed, when $t \rightarrow +\infty$, we have $\bar{h}^{(0)}(t) \rightarrow 0$, so that $v \rightarrow +\infty$ and $e^{-vn^2} \rightarrow 0$ in Eq.(55), leading to Eq.(53).

In the regimes where the time t is not too short, so that long wavelength modes have enough time to develop, **but is also** not too large, so that the equilibrium roughness is not reached, we obtain the usual Edwards-Wilkinson scaling [24]

$$\langle W_\Sigma^2 \rangle \simeq \Omega \left(\frac{\Omega c_{\text{eq}}^{(0)}}{1/\nu + \bar{h}^{(0)}(0)/D} \frac{8t}{\pi\Gamma} \right)^{1/2}, \quad (57)$$

which is associated to close-to-equilibrium roughening [24, 25]. The derivation of this expression is reported in Appendix B.

This expression is seen to provide a fair approximation of the evolution of $\langle W_\Sigma^2 \rangle$ for small deposition fluxes F and slow attachment-detachment kinetics as seen from Fig. 4. However, note that the expressions Eq.(55,57) become less accurate as attachment-detachment kinetics becomes faster, as seen from Fig. 5. Indeed, in the regime of fast attachment-detachment kinetics, one cannot neglect the dependence of the perturbation growth rate $\lambda_{\Sigma q}$ in the deposition rate F .

E. Peak of roughness for fast growth

During faster growth, the initial increase of the roughness is dominated by non-equilibrium effects, which consist of two contributions: (i) non-equilibrium fluctuations

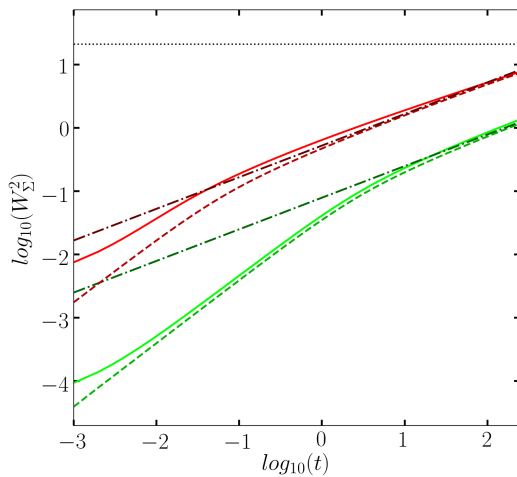


FIG. 5. Roughness at short and intermediate times for slow deposition fluxes. Solid curves: full numerical solution of the model Eq. (48); Dashed curves: long-wavelength approximation Eq. (55); Dash-dotted curves: Edwards-Wilkinson scaling Eq. (57). Kinetic coefficients: $\nu = 10^2$ (red) and $\nu = 1$ (green). The other model parameters are: $\Omega = 1$, $D = 10^4/4$, $c_{\text{eq}}^0 = 10^{-2}$, $\Gamma = 4.05$, $L = 512$, $\bar{h}^{(0)}(0) = 32$, and $F = 10^{-4}$.

associated to the deposition noise φ and (ii) the deterministic Mullins-Sekerka instability corresponding to positive $\lambda_{\Sigma q}$ or $\lambda_{\Delta q}$. These contributions produce roughness at short and finite wavelengths. However, such wavelengths are strongly suppressed during the collision. Indeed, growth is then slower in the late stages of the dynamics, and the line stiffness drives the system towards an equilibrium state where the power-spectrum [Eq.(44)] is dominated by long wavelength modes. As a consequence of the suppression of the short wavelength modes during the collision, the roughness decreases sharply, giving rise to a maximum of roughness for fast growth, as reported in Fig. 3.

Estimates of the time t_c at which the peak of roughness occur can be obtained in the limits of slow and fast attachment-detachment kinetics.

When the attachment-detachment kinetics is slow, the roughening is dominated by statistical fluctuations. Neglecting the contribution related to equilibrium fluctuations in the right-hand-side of Eq.(50) and considering that the roughness is dominated by short-wavelength modes around the value of the microscopic cutoff $q_c = \pi/a$, we find that

$$t_{\text{peak}} = \frac{1}{\Omega F - 2\nu\Gamma c_{\text{eq}}^0 \pi^2} \ln \left(\frac{\Omega F}{2\nu\Gamma c_{\text{eq}}^0 \pi^2} \right). \quad (58)$$

The details of this calculation are reported in Appendix D.

In contrast, for the regime of fast attachment-detachment kinetics, we assume that the roughening is dominated by the Mullins-Sekerka instability. We therefore associate t_c to the last time where the instability is present. As discussed above, the instability disappears

when the distance between the two interfaces decreases. In Fig. 2, we see that the instability disappears when the growth rate of the sum-mode $\lambda_{\Sigma q}$ changes sign at long-wavelength (i.e., small q). From an expansion of $\lambda_{\Sigma q}$ at $q \rightarrow 0$, we find that the instability disappears when $\bar{h}^{(0)}(t)$ becomes smaller than $\bar{h}^{(0)}(t_c) = (3c_{\text{eq}}^0 \Gamma D/F)^{1/3}$. Using Eq.(12), this corresponds to

$$t_c = \frac{1}{3\Omega F} \ln \left(\frac{F h_0^{(0)3}}{3c_{\text{eq}}^0 D \Gamma} \right). \quad (59)$$

As reported in Fig. 6, the values of the time of the peak t_c obtained from the full numerical simulations of the Langevin model at large deposition flux F are in good agreement with Eq.(58) for slow attachment-detachment kinetics, and with Eq.(59) for fast attachment-detachment kinetics.

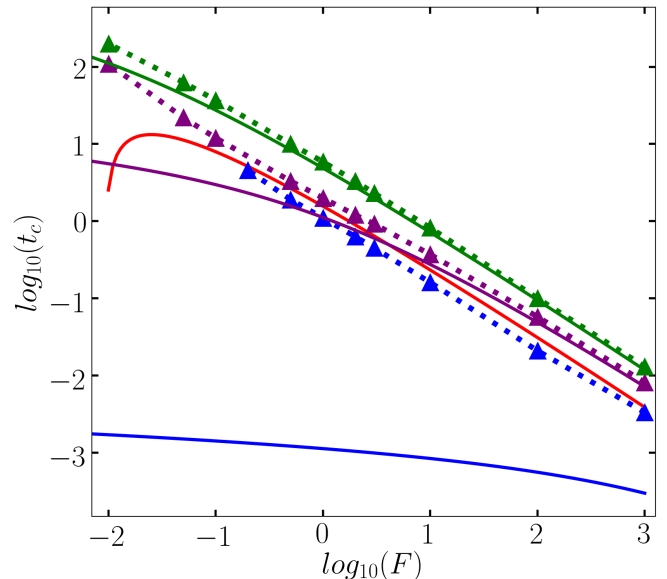


FIG. 6. Time of the peak of roughness as a function of the flux F . The triangles (joined by dotted lines) are extracted from the numerical solution of the full model: $\nu = 10^{-2}$ (green), $\nu = 1$ (violet), and $\nu = 10^4$ (blue). Solid curves with the same colors correspond to approximate expressions suitable for the fluctuation dominated regime Eq.(58). The red solid curve reports the approximate expression Eq.(59) for the instability-dominated regime. The other model parameters are: $\Omega = 1$, $D = 10^4/4$, $c_{\text{eq}}^0 = 10^{-2}$, $\Gamma = 4.05$, $L = 512$, and $\bar{h}^{(0)}(0) = 32$.

F. Classification of the roughening regimes

In this section, we wish to identify the different regimes for the evolution of the roughness as a function of relevant physical parameters. In order to identify the contributions which dominate the evolution of the roughness, we analyse the evolution of the ratio of the deterministic

term over the stochastic one in Eq. (50):

$$R_{\Sigma}(t) = \frac{\sum_{n \neq 0} 2\lambda_{\Sigma q}(t) \langle |\Sigma h_q^{(1)}(t)|^2 \rangle}{\sum_{n \neq 0} (B_{\Sigma q}(t) + 2\Omega^2 F \bar{h}^{(0)}(t)) L}. \quad (60)$$

where we recall that $q = 2\pi n/L$ and L is the system size along x . The denominator of R_{Σ} is always positive. Thus, the sign of the numerator dictates the sign of R_{Σ} . The special value $R_{\Sigma} = -1$ corresponds to $\partial_t \langle |\Sigma h_q^{(1)}(t)|^2 \rangle = 0$ from Eq. (50). The equilibrium state which is always obtained at long times obeys this condition. Therefore, R_{Σ} always converge to -1 at long times, i.e., when $t \rightarrow \infty$. When R_{Σ} crosses the line $R_{\Sigma} = -1$ at finite times, the roughness reaches an extremum, which is either a maximum or a minimum of W_{Σ}^2 . In addition, R_{Σ} can be positive only if $\lambda_{\Sigma q}(t) > 0$ for some value of q , i.e., only in the presence of the Mullins-Sekerka instability.

We define three regimes corresponding to the different types of dynamics resulting from the Langevin model. First, the monotonic roughening regime is observed in the absence of deterministic Mullins-Sekerka instability. We therefore have $\lambda_{\Sigma q}(t) < 0$ for all q and as a consequence $R_{\Sigma} < 0$. Hence, if $0 < R_{\Sigma} < -1$ at all times, then the dynamics is considered to be in the monotonic roughening regime. Second, the instability-dominated peak regime is defined as the regime where $R_{\Sigma} > 1$ at some point during the dynamics, i.e. when the instability contribution is larger than the noise contribution in Eq.(50). Third, when $R_{\Sigma} < 1$ and R_{Σ} crosses the line at $R_{\Sigma} = -1$, we consider that the dynamics belong to the fluctuation-dominated peak regime.

Some examples of dynamics in these three different regimes are reported in Fig. 7. The vertical dash-dotted lines mark the local extrema of the roughness. They coincide with the condition $R_{\Sigma} = -1$.

The occurrence of these regimes as a function of F/D and ν/D is summarized in Fig. 8. We observe that the boundary between the monotonous roughening regime and the fluctuation-dominated peak regime for low attachment/detachment kinetics is linear at small F/D and small ν/D , while the boundary between the monotonous roughening regime and the instability-dominated peak regime corresponds to a constant F/D .

IV. KINETIC MONTE-CARLO SIMULATIONS

A. KMC model

In this section, we present the lattice KMC model that is discussed in details in Ref. [19], and compare the simulation results with the Langevin model discussed above. The model is defined in a square lattice with two solids with initially flat interfaces located at $y = -d_0$ (interface $-$) and $y = +d_0$ (interface $+$). The length of each interface is L and periodic boundaries are considered in the x direction. Each atom of the solid is represented by a solid site (also called solid particle). The model is

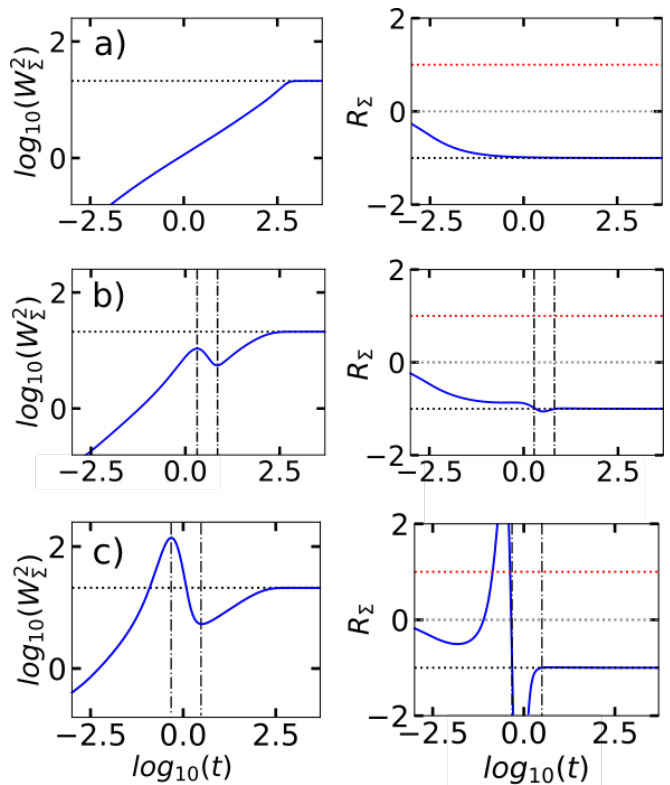


FIG. 7. Time evolution of W_{Σ}^2 and R_{Σ} . R_{Σ} is defined in (60) as the amplitude of the ratio of the deterministic part over the stochastic one. It gives a criterion for the domain classification in the phase diagram Fig. 8. The vertical dash-dotted lines mark the local extrema of the roughness. They coincide with the events $R_{\Sigma} = -1$. We have used the following model parameters: $\nu/D = 0.4$, $\Omega = 1$, $D = 10^4/4$, $c_{\text{eq}}^0 = 10^{-2}$, $\Gamma = 4.05$, $L = 512$, $\bar{h}^{(0)}(0) = 32$. a) $F/D = 1.2 \cdot 10^{-3}$. b) $F/D = 2.0 \cdot 10^{-4}$. c) $F/D = 2.0 \cdot 10^{-6}$.

represented in Fig 9. We use the lattice parameter a as the unit length. As a consequence, the atomic area is $\Omega = a^2 = 1$.

Deposition events occur only in the region between the two solid interfaces. The external particle flux is F , measured in number of incident particles per site per unit time. If an incident particle is deposited on a free site, it becomes a mobile particle; otherwise, the deposition attempt is rejected. The number of random hops of a mobile particle to nearest neighbor sites per unit time is D' and excluded volume conditions are applied (i.e. hop attempts to occupied sites are rejected). The corresponding tracer diffusion coefficient of an isolated particle in two dimensions is $D = D'/4$.

For each value of the horizontal coordinate x , the top (bottom) solid particle at the $-$ ($+$) interface can detach with rate $Q\epsilon^n$, where n is the number of nearest neighbors and $\epsilon < 1$; thus, weakly bonded solid particles detach with higher probability than strongly bonded ones. Solid particles that detach from the solid become mobile particles. A mobile particle that has at least one

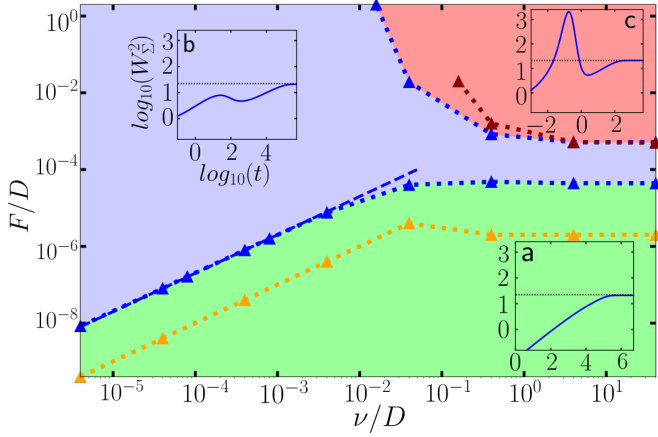


FIG. 8. Phase diagram reporting the three main regimes in the $(F/D, \nu/D)$ plane. The blue triangles define the boundaries of the three regions. The green region corresponds to the monotonic roughening regime. The blue region corresponds to the presence of a peak of roughness dominated by out-of-equilibrium fluctuations. The red region corresponds to the presence of a peak of roughness due to a morphological instability. The orange and red triangles respectively correspond to the regions where $W^2 \propto t^{1/2}$ and where W^2 grows faster than t^2 . The parameters of the insets are: a) $F/D = 4.10^{-8}$, $\nu/D = 4.10^{-4}$; b) $F/D = 4.10^{-5}$, $\nu/D = 4.10^{-3}$; c) $F/D = 4.10^{-3}$, $\nu/D = 4.10^{-1}$. The other model parameters are: $\Omega = 1$, $D = 10^4/4$, $c_{\text{eq}}^0 = 10^{-2}$, $\Gamma = 4.05$, $L = 512$, $\bar{h}^{(0)}(0) = 32$.

nearest neighbor with the $-$ interface and is at the lowest possible position above the bottom solid may attach and become a solid particle. With this rule, no overhang of the $-$ interface can be formed. Hence, our description of the interfaces enter into the class of Solid-On-Solid (SOS) models. A similar rule is applied on the $+$ interface. The attachment rate is Q . Hence, in contrast to detachment, attachment does not depend on the local configuration of the interface.

The parameter ϵ is linked to the bond energy J

$$\epsilon = \exp[-J/k_B T], \quad (61)$$

We can therefore rewrite the detachment rate as $Q\epsilon^n = Q \exp[-nJ/k_B T]$. Recalling that the attachment rate is Q , we recover the usual SOS bond-breaking model (and its mapping to the Ising model) [6, 26] with bond energy J and equilibrium concentration

$$c_{\text{eq}} = \exp[-2J/k_B T] = \epsilon^2.$$

In addition, the line stiffness of SOS one-dimensional edges reads [6]

$$\tilde{\gamma} = \frac{k_B T}{2\Omega^{1/2}} (\epsilon^{-1/4} - \epsilon^{1/4})^2. \quad (62)$$

Furthermore, the attachment-detachment kinetic constant is [26]

$$\nu = Q.$$

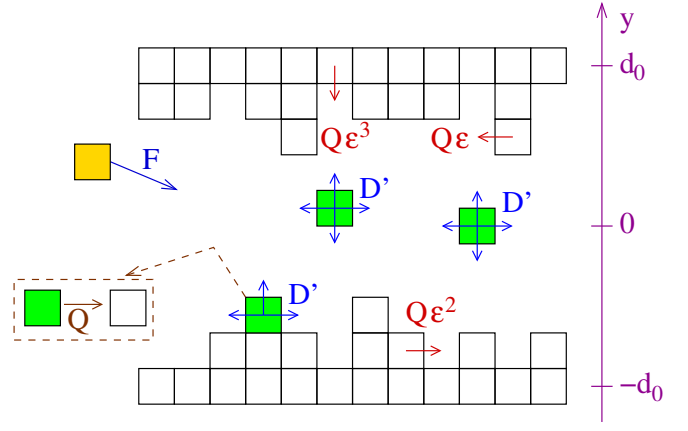


FIG. 9. Schematic of the KMC model. Solid particles are in white, mobile particles in green, and an incident particle is shown in yellow. Blue arrows indicate deposition events and the possible hops of mobile particles. Red arrows indicate detachment of solid particles. The brown arrow shows the transformation of a mobile particle into a solid particle at its current position. The corresponding rates are indicated near the arrows.

B. Regimes observed in simulations

Simulations with $L = 512$ and $d_0 = 32$ are reported in Fig. 10 for $\epsilon = 10^{-2}$ and 10^{-1} . Using Eq. (62), these values of ϵ correspond respectively to $\Gamma = 4.05$ used in all figures of Section II, and to $\Gamma = 0.74$. The general scenario for the evolution of the roughness is seen to be in qualitative agreement with the results of the Langevin model. Indeed, for slow growth, we obtain a roughness W_Σ^2 that increases monotonically with time, and then saturates at long times at an equilibrium value. In contrast, faster growth leads to the formation of a peak of roughness. Furthermore, the distance-roughness W_Δ^2 follows the roughness W_Σ^2 at short times and then decreases sharply during the collision as in the Langevin model. The overall scenario is seen clearly for $\epsilon = 10^{-1}$, but KMC simulations are too slow to reach the asymptotic equilibrium roughness when $\epsilon = 10^{-2}$.

In all plots, the dashed lines are guides to the eye for a power-law behavior of the squared roughness with the indicated exponent. If the exponent before the maximum exceeds 2 during some time interval, the system is considered to be unstable. Indeed, the amplitudes can grow faster than linearly in the presence of a Mullins-Sekerka instability. In contrast, when the exponent is near $1/2$, we recover the quasi-equilibrium EW growth, which is discussed in Sec.III D. In Fig. 8, this simple criterion based on the exponent of the power-law before the peak in the Langevin model is shown in orange and red triangles. This criterion is seen to lead qualitatively to the same three regions as the criterion based on the evolution of $R_\Sigma(t)$ discussed in Section III F (examples of comparison of power laws with the results of the Langevin model are reported in Appendix in Fig. 16).

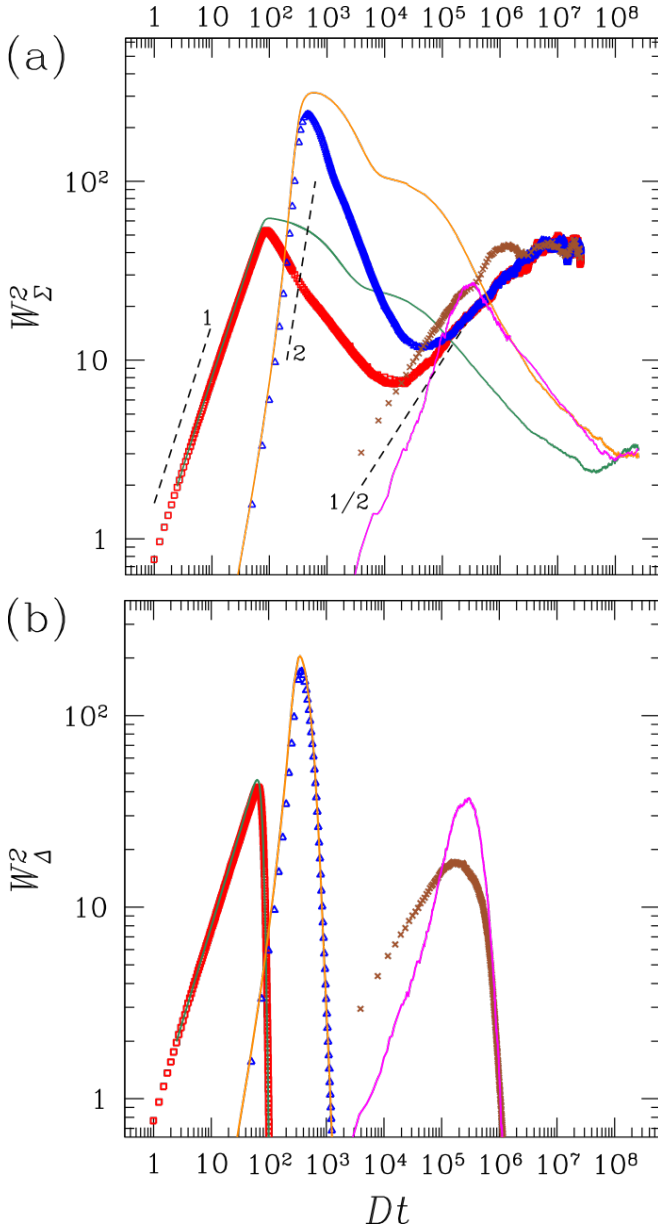


FIG. 10. Temporal evolution of the roughness in KMC simulations. (a) W_Σ^2 and (b) W_Δ^2 as a function of Dt for several flux-diffusion ratios: $F/D = 40$ [$\epsilon = 0.1$ (red), $\epsilon = 0.01$ (green)]; $F/D = 4 \times 10^{-3}$ [$\epsilon = 0.1$ (blue), $\epsilon = 0.01$ (orange)]; $F/D = 4 \times 10^{-6}$ [$\epsilon = 0.1$ (brown), $\epsilon = 0.01$ (magenta)]. The other parameters are $Q/D = 0.4$, $d_0 = 32$, and $L = 512$. The KMC simulation data of these graphs are from Ref. [19].

Based on this classification with exponents, a phase diagram is also drawn for KMC simulations with $\epsilon = 10^{-1}$ in Fig. 11. The KMC simulations lead to the same three regions as the phase diagram Fig. 8, with qualitative but not precise quantitative agreement. However for KMC simulations, we also observe a different region for high fluxes, which corresponds to a situation where almost all sites on the substrate in the gap between the two edges are covered by atoms. In this high-coverage regime, the

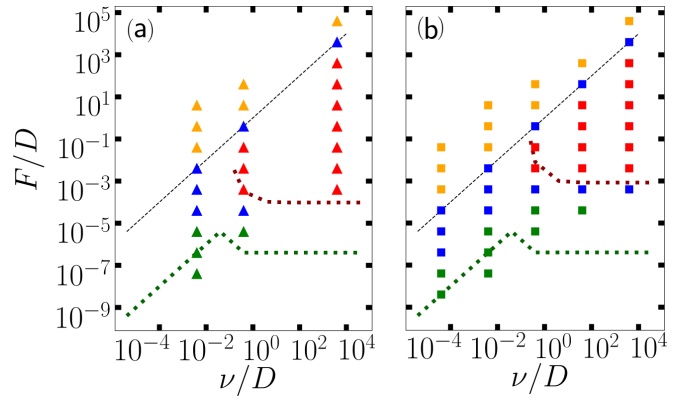


FIG. 11. Phase diagram from KMC and comparison with the Langevin model. The symbols represent the regimes identified in KMC simulations. The dotted lines represent the predictions of the Langevin model. The dashed line indicates the condition $F/Q = 1$. (a) $h_0 = 32$ and (b) $h_0 = 16$. Other parameters: $\epsilon = 10^{-1}$, $L = 512$. The KMC simulation data of these graphs are from Ref. [19].

exponent before the maximum is near 1, and the roughening regime is therefore classified as being random deposition (RD)[24] as already discussed in Sec. III B.

This regime of high coverage is obtained when the coverage close to the edges becomes of the order of 1. Using the quasistatic expression of the concentration at the edges Eq. (9) we obtain a condition for being in the low-coverage regime $\Omega c \ll 1$, leading to $\Omega F \ll \nu/\bar{h}_0^{(0)}(0)$. This condition is qualitatively correct, but quantitatively not in agreement with the transition to the high-coverage regime in Fig. 11. Indeed, the quasistatic concentration only provides an upper bound for the possible value of the coverage at the edge. A simple condition comparing deposition and attachment $F/Q < 1$ is seen to be in better agreement with the simulations, suggesting as expected, that strong non-quasistatic effects come to the fore where the concentration is not small.

C. EW regime at low coverage

In the regime of low coverages, the EW scaling can be observed. Using Eqs. (57) and (62), we obtain

$$W_\Sigma^2 = \frac{4}{\pi^{1/2}} \frac{\epsilon}{\epsilon^{-1/4} - \epsilon^{1/4}} (Qt)^{1/2}. \quad (63)$$

This expression is valid in the limit $\bar{h}_0^{(0)} Q/D \ll 1$, which corresponds to our KMC simulations.

In Fig. 12, the ratio $W_\Sigma^2/(Qt)^{1/2}$ is seen to reach 0.12 ± 0.02 for a wide range of parameters. Using Eq. (63) with $\epsilon = 10^{-1}$, we find $W_\Sigma^2/(Qt)^{1/2} \approx 0.18$. Once again, the predictions are providing the correct order of magnitude, but do not reach precise quantitative agreement. This difference between the KMC simulations and the predictions of the Langevin model could be caused by

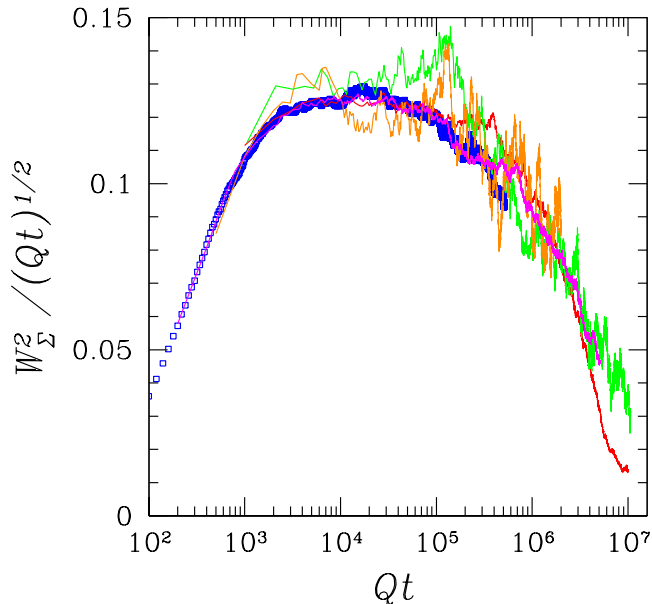


FIG. 12. Evaluation of the prefactor in the Edwards-Wilkinson scaling of the roughness. In all cases, $\epsilon = 0.1$ and $L = 512$. Other parameters: $(F/D, \nu/D, d_0) = (4 \times 10^{-10}, 4 \times 10^{-4}, 64)$ blue squares; $(4 \times 10^{-9}, 4 \times 10^{-3}, 32)$ red curve; $(4 \times 10^{-10}, 4 \times 10^{-3}, 32)$ green curve; $(4 \times 10^{-10}, 4 \times 10^{-3}, 32)$ green curve; $(4 \times 10^{-9}, 4 \times 10^{-3}, 64)$ orange curve; $(4 \times 10^{-10}, 4 \times 10^{-3}, 64)$ magenta curve.

the inaccuracy of the equilibrium line stiffness Eq. (62) in non-equilibrium growth conditions, as discussed in other models e.g. in Refs. [27, 28].

D. Discussion

Some features of the KMC simulations are more delicate to compare to the Langevin model. For example, the comparison of the short time behaviors is difficult. A first reason for this difficulty is that the short time behavior $W^2 \sim t$ analyzed in Section III B crucially depends on the details of the atomic cutoff. In addition, the KMC simulations were started with no atom in the gap. The initial build-up of the concentration up to the quasistatic profile Eqs. (8) and (9) is not described in the Langevin model. In contrast, the Langevin model assumes an initial condition that starts with the quasistatic profile. Hence, we have not tried to compare the short time behavior in KMC and Langevin model.

Another difference is the quantitative value of the equilibrium asymptotic roughness at long times. Indeed, the Langevin model assumes that the free energy of the grain boundary is simply the sum of the free energies of the two edges. This assumption discards the entropic cost of bringing the two interfaces close to each other. Such a reduction of the entropy leads to a larger line tension,

and therefore to a larger stiffness of the grain boundary. This increase of the stiffness in turn leads to a decrease of the equilibrium roughness. A quantitative analysis of this effect is reported in [19].

Despite these limitations in the comparison with KMC simulations, the Langevin model is seen to be able to recover the important and generic features of grain boundary formation, i.e. the possible non-monotonic behavior of the roughness with a peak and a minimum, and the generic competition between statistical fluctuations and instabilities for the production of roughness.

V. CONCLUSION

In summary, we have presented a Langevin model which aims at describing the formation of grain boundaries in 2D materials. Previous development of Langevin models has already proved useful to describe asymptotic power-law behaviors of the roughness of one-dimensional interfaces such as atomic steps [16] during growth or at equilibrium. However, the formation of grain boundaries is a challenging problem because it involves transient phenomena occurring in finite time. A first advance in the modeling of grain boundaries [5] has allowed one to model the collision of two interfaces in the presence of short-range interactions. The addition of long-range interactions and fluctuations associated with the diffusion of growth units allows one to get closer to existing experimental conditions, but leads to additional technical difficulties. Indeed, fluctuations emerge as perturbations of a time-dependent reference state that describes the closing of the gap between two 2D materials governed by the Zeno effect.

The Langevin model presented in this paper aims at tackling this challenging problem. This model allows one to identify prominent features in the formation of grain boundaries associated to statistical fluctuations and instabilities. We find that fast-enough growth is accompanied with a non-monotonous behaviour of the roughness as a function of time, with a peak and a minimum before the slow relaxation of the grain boundary after collision towards its equilibrium roughness. The competition between diffusion-limited instabilities and statistical noise for the production of the roughness gives rise to distinctive regimes that can be summarized in a phase diagram. A quantitative comparison of these results with KMC simulations reported in Ref. [19] is encouraging and suggests that our results could serve as a guide to understand the effect of various physical parameters in experiments.

Appendix A: Deposition noise

The goal of this Appendix A is to determine the amplitudes of the out-of-equilibrium fluctuations in Eq. (39). We consider a discrete one-dimensional model with two edges growing towards each other via the deposition of

particles in continuous time. We then determine the amplitude of the Langevin forces in a continuum model that are consistent with the 1D discrete model.

1. One-dimensional lattice model

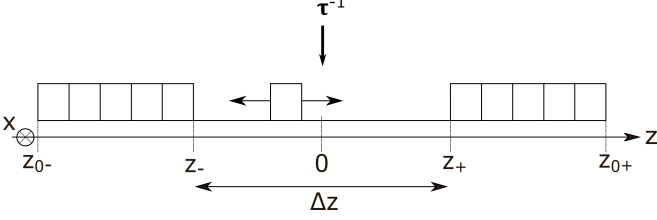


FIG. 13. Two flat bidimensional edges represented as two facing lines as the information along the transversal axis is irrelevant.

The 1D model is composed of two edges defined by their position z_+ and z_- along the z -axis, as described on Fig. 13. Deposited particles diffuse along z , and attach to one of the edges. We consider the limit of low deposition flux, where each deposited particle attaches to one of the edges before another particle has landed. Since particles are deposited at a random position in the gap, the deposition-diffusion-attachment process leads to random incorporation of particles to the left or to the right with a probability $p = 1/2$. In the spirit of the quasistatic approximation in the main text, and discarding the possibility of slow attachment kinetics, we assume that the process of diffusion and attachment is instantaneous.

Since we focus on the noise related to freshly landed atoms, we assume that particles never detach from the edges. Thus, only one of the two following deposition events can occur:

$$z_- \rightarrow z_- + 1, \quad (\text{A1})$$

$$z_+ \rightarrow z_+ - 1. \quad (\text{A2})$$

These two events can be written in terms of the in-phase and out-of-phase modes

$$\Delta z = z_+ - z_- \rightarrow \Delta z - 1, \quad (\text{A3})$$

$$\Sigma z = z_+ + z_- \rightarrow \Sigma z \pm 1. \quad (\text{A4})$$

The number of empty sites is equal to Δz . We denote m_+ as the number of atoms deposited on the $+$ side, m_- on the $-$ side, and $\Sigma m = m_+ + m_-$ the total number of deposited atoms. We assume a left-right symmetric initial condition with $z_{0+} = -z_{0-} = \Delta z_0/2$, and $\Sigma z_0 = 0$, where Δz_0 is the initial number of free sites. We therefore have $z_- = z_{0-} + m_-$ and $z_+ = z_{0+} - m_+$. This leads to a simple bijective relation between Δz and Σm , and between Σz and Δm :

$$\Delta z = \Delta z_0 - \Sigma m, \quad (\text{A5})$$

$$\Sigma z = \Sigma z_0 - \Delta m = -\Delta m. \quad (\text{A6})$$

Each site in the gap between the two edges can be filled with a rate τ^{-1} . The evolution of Δz depends only on the number of deposition events, and does not depend on the fact that particles are attached to the left or to the right. Hence, the evolution of Δz can be derived from a direct analogy to a decay process, where a number Δz of independent empty sites can be filled by a particle with a rate τ^{-1} . Let $w(t)$ be the probability for a given site to be empty up to a time t

$$dw(t) = -w(t) \frac{dt}{\tau} \Leftrightarrow w(t) = e^{-\frac{t}{\tau}}. \quad (\text{A7})$$

The probability for Δz sites to be empty at a given time t is

$$P(\Delta z, t) = \binom{\Delta z_0}{\Delta z} w^{\Delta z} (1-w)^{\Delta z_0 - \Delta z}, \quad (\text{A8})$$

which leads to the average number of free sites

$$\begin{aligned} \langle \Delta z \rangle_t &= \sum_{\Delta z} \binom{\Delta z_0}{\Delta z} w^{\Delta z} (1-w)^{\Delta z_0 - \Delta z} \Delta z, \\ \langle \Delta z \rangle_t &= w \Delta z_0 = \Delta z_0 e^{-\frac{t}{\tau}}. \end{aligned} \quad (\text{A9})$$

One retrieves the Zeno effect with the exponential decrease of the gap as in Eq. (12). The second moment of Δz is given by

$$\begin{aligned} \langle \Delta z^2 \rangle_t &= \sum_{\Delta z} \binom{\Delta z_0}{\Delta z} w^{\Delta z} (1-w)^{\Delta z_0 - \Delta z} (\Delta z)^2, \\ &= w(1-w) \Delta z_0 + \Delta z_0^2 w^2, \end{aligned} \quad (\text{A10})$$

which leads to the following variance

$$V_{\Delta} = \langle \Delta z^2 \rangle_t - \langle \Delta z \rangle_t^2 = \Delta z_0 e^{-\frac{t}{\tau}} \left(1 - e^{-\frac{t}{\tau}}\right). \quad (\text{A11})$$

In the following, we write the properties of Σz as a function of Δz . Since Δz monotonously decreases with time, one can directly switch from expected values at fixed t to expected values at fixed Δz . The probability of Σz given a value of Δz is denoted $P(\Sigma z | \Delta z)$, and the expectation value for a given Δz is denoted as $\langle \cdot \rangle_{\Delta z}$. We start with the law of total probability

$$P(\Sigma z, t) = \sum_{\Delta z=0}^{\Delta z_0} P(\Sigma z | \Delta z) P(\Delta z, t). \quad (\text{A12})$$

The n -th moment of Σz at t is written as

$$\begin{aligned} \langle (\Sigma z)^n \rangle_t &= \sum_{\Sigma z} (\Sigma z)^n P(\Sigma z, t) \\ &= \sum_{\Delta z=0}^{\Delta z_0} P(\Delta z, t) \langle (\Sigma z)^n \rangle_{\Delta z}. \end{aligned} \quad (\text{A13})$$

where

$$\langle (\Sigma z)^n \rangle_{\Delta z} = \sum_{\Sigma z} (\Sigma z)^n P(\Sigma z | \Delta z). \quad (\text{A14})$$

Since $\Sigma z = \Sigma m - 2m_+$, we will evaluate the moments of m_+

$$\langle m_+^n \rangle_{\Delta z} = \sum_{m_+} m_+^n P(m_+ | \Delta z). \quad (\text{A15})$$

The probability of m_+ particles attached to + side among Σm particles deposited is

$$P(m_+ | \Delta z) = P(m_+ | \Sigma m) = \frac{1}{2^{\Sigma m}} \binom{\Sigma m}{m_+}. \quad (\text{A16})$$

One obtains from (A15) for $n=1$ and $n=2$:

$$\langle m_+ \rangle_{\Delta z} = \sum_{m_+} m_+ P(m_+ | \Delta z) = \frac{1}{2} \Sigma m, \quad (\text{A17})$$

$$\langle m_+^2 \rangle_{\Delta z} = \sum_{m_+} m_+^2 P(m_+ | \Delta z) = \frac{1}{4} \Sigma m + \frac{1}{4} (\Sigma m)^2, \quad (\text{A18})$$

which finally leads to

$$\langle \Sigma z \rangle_{\Delta z} = \Sigma m - 2 \langle m_+ \rangle_{\Delta z} = 0, \quad (\text{A19})$$

$$\langle (\Sigma z)^2 \rangle_{\Delta z} = \langle (\Sigma m - 2m_+)^2 \rangle_{\Delta z} = \Sigma m. \quad (\text{A20})$$

From Eq. (A13), the average vanishes

$$\langle \Sigma z \rangle_t = 0. \quad (\text{A21})$$

Moreover, the variance is obtained by inserting A20 using Eq. (A5) into Eq. (A13)

$$\begin{aligned} V_\Sigma &= \langle (\Sigma z)^2 \rangle_t = \sum_{\Delta z=0}^{\Delta z_0} P(\Delta z, t) \langle (\Sigma z)^2 \rangle_{\Delta z} \\ &= \Delta z_0 \left(1 - e^{-\frac{t}{\tau}} \right). \end{aligned} \quad (\text{A22})$$

2. Langevin model

We now design continuum Langevin equations which are consistent with (A11) and (A22). The position along the x -axis parallel to the edge is here explicitly expressed by the discrete index m . We assume that the process Δz_m and Σz_m at a given m is independent from the others. This means physically that we assume that attachment occurs at the same coordinate x as the deposition event. The decrease of the distance between the two edges Δz is taken to be proportional to the deposition rate as in (A9):

$$\partial_t \Delta z_m = -\frac{1}{\tau} \Delta z_m + \tilde{\varphi}_{\Delta, m}(t), \quad (\text{A23})$$

$$\partial_t \Sigma z_m = \tilde{\varphi}_{\Sigma, m}(t). \quad (\text{A24})$$

The Langevin forces have zero average $\langle \tilde{\varphi}_{\Delta, m}(t) \rangle = \langle \tilde{\varphi}_{\Sigma, m}(t) \rangle = 0$. They are also uncorrelated in time, and their amplitudes are defined as

$$\langle \tilde{\varphi}_{i, m}(t_1) \tilde{\varphi}_{j, m'}(t_2) \rangle = 2\tilde{D}_{i, m}(t_1) \delta(t_1 - t_2) \delta_{m, m'} \delta_{i, j}, \quad (\text{A25})$$

where i and j are either Δ or Σ , where $\delta_{n, n'}$ is the Kronecker delta symbol. The equations (A23) and (A24) are solved as

$$\Delta z_m(t) = \Delta z_{0, m} e^{-t/\tau} + \int_0^t dt_1 \tilde{\varphi}_{\Delta, m}(t_1) e^{\frac{1}{\tau}(t_1 - t)}, \quad (\text{A26})$$

$$\Sigma z_m(t) = \int_0^t dt_1 \tilde{\varphi}_{\Sigma, m}(t_1) e^{\frac{1}{\tau}(t_1 - t)}. \quad (\text{A27})$$

This leads to $\langle \Delta z_m \rangle_t = \Delta z_{0, m} e^{-t/\tau}$ and $\langle \Sigma z_m \rangle_t = 0$, in agreement with Eqs. (A9) and (A21). The variances in the Langevin model read

$$V_\Delta = \langle (\Delta z_m)^2 \rangle_t - \langle \Delta z_m \rangle_t^2 = \int_0^t dt_1 2\tilde{D}_{\Delta, m} e^{\frac{2}{\tau}(t_1 - t)}, \quad (\text{A28})$$

$$V_\Sigma = \langle (\Sigma z_m)^2 \rangle_t = \int_0^t dt_1 2\tilde{D}_{\Sigma, m}(t_1). \quad (\text{A29})$$

We then impose the expression of $\tilde{D}_{\Delta, m}$ and $\tilde{D}_{\Sigma, m}$ to obtain agreement with (A11) and (A22):

$$2\tilde{D}_{\Delta, m}(t) = 2\tilde{D}_{\Sigma, m}(t) = \frac{1}{\tau} \langle \Delta z_m \rangle_t. \quad (\text{A30})$$

Indeed, using these expressions, we find

$$V_\Delta = \int_0^t dt_1 \frac{1}{\tau} \langle \Delta z_m \rangle_{t_1} = \Delta z_{0, m} e^{-\frac{t}{\tau}} \left(1 - e^{-\frac{t}{\tau}} \right), \quad (\text{A31})$$

$$V_\Sigma = \int_0^t dt_1 \frac{1}{\tau} \langle \Delta z_m \rangle_{t_1} = \Delta z_{0, m} \left(1 - e^{-\frac{t}{\tau}} \right). \quad (\text{A32})$$

We now take the continuum limit. Multiplying Eqs. (A23, A24) by the atomic length a , letting $a \rightarrow 0$, and using $a\Delta z_m \rightarrow \Delta h(x, t)$, $a\Sigma z_m \rightarrow \Sigma h(x, t)$ and $a\tilde{\varphi}_{i, m}(t) \rightarrow \varphi_i(x, t)$ leads to

$$\partial_t \Delta h(x, t) = -\frac{1}{\tau} \Delta h(x, t) + \varphi_\Delta(x, t), \quad (\text{A33})$$

$$\partial_t \Sigma h(x, t) = \varphi_\Sigma(x, t), \quad (\text{A34})$$

and using $\delta_{m, m'} \rightarrow a \delta(x - x')$, we find

$$\langle \varphi_i(x, t) \varphi_j(x', t') \rangle = A_i(x, t) \delta(x - x') \delta(t - t') (2\pi)^2 \delta_{i, j}. \quad (\text{A35})$$

where

$$\begin{aligned} A_\Sigma(x, t) &= 2\tilde{D}_\Sigma(t) a^3, \\ A_\Delta(x, t) &= 2\tilde{D}_\Delta(t) a^3. \end{aligned} \quad (\text{A36})$$

Finally, using Eq. (A30) and the relations $1/\tau = \Omega F$ and $a \langle \Delta z_m \rangle_t \rightarrow 2\bar{h}^{(0)}(t)$, we obtain

$$A_\Delta(x, t) = A_\Sigma(x, t) = 2\Omega^2 F \bar{h}^{(0)}(t), \quad (\text{A37})$$

which is identical to (39).

Appendix B: Close-to-equilibrium roughening

In this appendix, we provide a derivation of the evolution of the roughness in the limit of small incoming flux $F \rightarrow 0$. We start with the evolution equation for the power-spectrum Eq.(50). Changing variables from t to $\bar{h}^{(0)}(t)$, we obtain

$$\begin{aligned} \partial_{\bar{h}^{(0)}} \langle |\Sigma h_q^{(1)}(t)|^2 \rangle = & -2 \frac{\lambda_{\Sigma q}}{\Omega F \bar{h}^{(0)}} \langle |\Sigma h_q^{(1)}(t)|^2 \rangle \\ & - \frac{B_{\Sigma q} L}{\Omega F \bar{h}^{(0)}} - 2\Omega L. \end{aligned} \quad (\text{B1})$$

Since long wavelength contributions dominate the roughness at equilibrium, we expect the roughening process to be dominated by long wavelength modes close to equilibrium. As a consequence, we take both limits $F \rightarrow 0$ and $q \rightarrow 0$ in the expressions of $\lambda_{\Sigma q}$ and $B_{\Sigma q}$, leading to

$$\begin{aligned} \Omega F \bar{h}^{(0)} \left(\bar{h}^{(0)} + \frac{D}{\nu} \right) \partial_{\bar{h}^{(0)}} \langle |\Sigma h_q^{(1)}(t)|^2 \rangle = & \\ 2\Omega D c_{\text{eq}}^{(0)} \Gamma q^2 \langle |\Sigma h_q^{(1)}(t)|^2 \rangle - 4\Omega^2 c_{\text{eq}}^{(0)} D L. \end{aligned} \quad (\text{B2})$$

Considering a flat initial condition $\langle |\Sigma h_q^{(1)}(0)|^2 \rangle = 0$, the solution of this equation reads

$$\langle |\Sigma h_q^{(1)}(t)|^2 \rangle = \frac{2\Omega L^3}{\Gamma(2\pi n)^2} (1 - e^{-vn^2}), \quad (\text{B3})$$

where

$$v = 2\Omega \Gamma \left(\frac{2\pi}{L} \right)^2 \frac{\nu c_{\text{eq}}^{(0)}}{\Omega F} \ln \frac{1 + \frac{D}{\nu \bar{h}^{(0)}(t)}}{1 + \frac{D}{\nu \bar{h}^{(0)}(0)}} > 0. \quad (\text{B4})$$

The Σ -roughness is then evaluated as

$$\langle W_{\Sigma}^2 \rangle = \frac{\Omega L}{2\pi^2 \Gamma} \sum_{n \neq 0} \frac{1}{n^2} (1 - e^{-vn^2}). \quad (\text{B5})$$

The Σ -roughness exhibits different behaviors when $v \gg 1$ and when $v \ll 1$. In the limit $v \gg 1$, the term e^{-vn^2} is negligible in Eq.(B5), and one obtains the expected asymptotic equilibrium value Eq.(53). In the opposite limit $v \ll 1$, the sum in Eq.(B5) can be approximated by an integral,

$$\begin{aligned} \langle W_{\Sigma}^2 \rangle & \approx \frac{\Omega L}{2\pi^2 \Gamma} 2 \int_1^{\infty} dn \frac{1}{n^2} (1 - e^{-vn^2}) \\ & \approx \frac{\Omega L}{2\pi^2 \Gamma} 2v^{1/2} \int_0^{\infty} dx \frac{1}{x^2} (1 - e^{-x^2}) \\ & = \frac{\Omega L}{2\pi^2 \Gamma} 2v^{1/2} \pi^{1/2}. \end{aligned} \quad (\text{B6})$$

where $x = vn^2$.

Care should be taken because the relation between v and t is nonlinear and depends on the attachment-detachment kinetics.

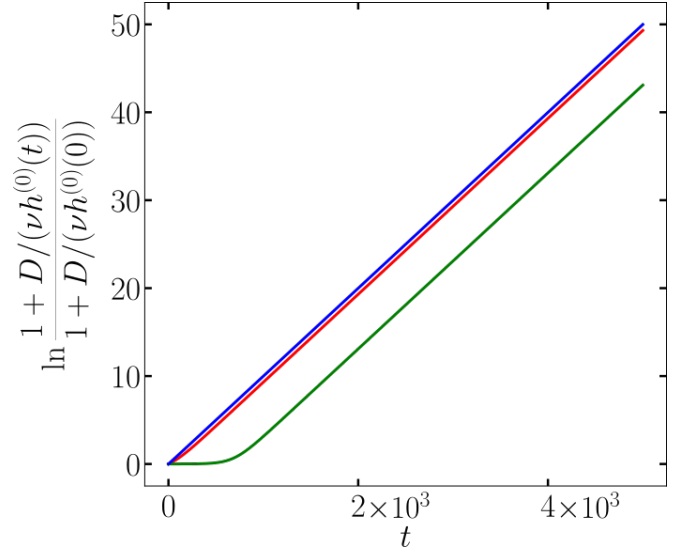


FIG. 14. The quantity $v \times 4\pi^2 F / (2\Gamma \nu c_{\text{eq}}^0 L^2)$ is plotted as a function of time for: $\nu \bar{h}^{(0)}(0)/D = 10^{-2}$ (blue), $\nu \bar{h}^{(0)}(0)/D = 1$ (red), and $\nu \bar{h}^{(0)}(0)/D = 10^3$ (green). The other model parameters are $\Omega = 1$, $D = 10^4/4$, $c_{\text{eq}}^0 = 10^{-2}$, $\Gamma = 4.05$, $L = 512$, $\bar{h}^{(0)}(0) = 32$, and $F = 10^{-2}$.

However, in general when $\Omega F t \ll 1$, then

$$v \approx 2\Omega \Gamma \left(\frac{2\pi}{L} \right)^2 \frac{\nu c_{\text{eq}}^{(0)} t}{1 + \nu \bar{h}^{(0)}(0)/D}. \quad (\text{B7})$$

Thus $v \ll 1$ corresponds to

$$t \ll \frac{1}{2\Omega c_{\text{eq}}^{(0)} \nu \Gamma} \left(\frac{L}{2\pi} \right)^2 \left(1 + \frac{\nu \bar{h}^{(0)}(0)}{D} \right) \quad (\text{B8})$$

In this regime where both $t \ll 1/(\Omega F)$ and the inequality (B8) are obeyed, Eq.(57) is obtained from the combination of Eqs.(B6,B7).

Appendix C: Short-time behavior

An expansion of the evolution equation for the roughness Eq. (48) to first order in $h^{(0)}(t) - h^{(0)}(0)$ leads to:

$$\begin{aligned} \langle W_{\Sigma}^2 \rangle & = -\frac{1}{L} \sum_{n \neq 0}^N (h^{(0)}(t) - h^{(0)}(0)) \left(\frac{B_{\Sigma q}(\bar{h}^{(0)})}{\Omega F \bar{h}^{(0)}} + 2\Omega \right) \\ & = (h^{(0)}(0) - h^{(0)}(t)) \frac{1}{L} \left[\sum_{n \neq 0}^N \frac{B_{\Sigma q}(\bar{h}^{(0)})}{\Omega F \bar{h}^{(0)}} + 4\Omega N \right]. \end{aligned} \quad (\text{C1})$$

The first term inside the brackets exhibits two limits for fast and slow attachment-detachment kinetics

$$\frac{B_{\Sigma q}(\bar{h}^{(0)})}{\Omega F \bar{h}^{(0)}} \xrightarrow{\nu/D \rightarrow +\infty} \frac{4\Omega c_{\text{eq}}^{(0)} D}{F \bar{h}^{(0)}} \frac{q}{\tanh k}, \quad (\text{C2})$$

$$\frac{B_{\Sigma q}(\bar{h}^{(0)})}{\Omega F \bar{h}^{(0)}} \xrightarrow{\nu/D \rightarrow 0} \frac{4\Omega c_{\text{eq}}^{(0)} D}{F \bar{h}^{(0)}} \frac{\nu}{D} = \frac{4\Omega c_{\text{eq}}^{(0)} \nu}{F \bar{h}^{(0)}}. \quad (\text{C3})$$

To calculate the sum over all modes of the last term, one recalls the discrete-continuum correspondences: $q = 2\pi n/L$ and $N = L/2a$, which give $dn = Ldq/2\pi$ and $q = \pi n/Na$. Besides, $k = q\bar{h}^{(0)}$, which leads to $dk = \bar{h}^{(0)}dq$ and $dn = L/(2\pi\bar{h}^{(0)})dk$. For $2\pi\bar{h}^{(0)}/L \ll 1$, we then have

$$\begin{aligned} \sum_{n \neq 0}^{|n| \leq N} \frac{k}{\tanh k} &\simeq \frac{L}{\pi \bar{h}^{(0)}} \int_{\frac{\pi}{2} \bar{h}^{(0)}}^{\pi \bar{h}^{(0)}} dk \frac{k}{\tanh k} \\ &\simeq \frac{L}{\pi \bar{h}^{(0)}} \int_0^{\pi \bar{h}^{(0)}} dk \frac{k}{\tanh k}. \end{aligned} \quad (\text{C4})$$

Since $\bar{h}^{(0)} \gg a$, we have $\tanh k \underset{k \gg 1}{\sim} 1$ and

$$\sum_{n \neq 0}^{|n| \leq N} \frac{q}{\tanh k} \simeq \frac{L}{\pi \bar{h}^{(0)} 2} \frac{1}{2} \left(\frac{\pi \bar{h}^{(0)}}{a} \right)^2 = \frac{L\pi}{2a^2}. \quad (\text{C5})$$

In the diffusion limited regime $\nu/D \rightarrow +\infty$, we obtain:

$$\langle W_{\Sigma}^2 \rangle_{\nu/D \rightarrow +\infty} \simeq \frac{2\Omega^2}{a} \left(c_{\text{eq}}^{(0)} \frac{\pi D}{a} + F \bar{h}^{(0)}(0) \right) t. \quad (\text{C6})$$

Similarly, for $\nu/D \rightarrow 0$:

$$\langle W_{\Sigma}^2 \rangle_{\nu/D \rightarrow 0} \simeq \frac{2\Omega^2}{a} \left(c_{\text{eq}}^{(0)} 2\nu + F \bar{h}^{(0)}(0) \right) t. \quad (\text{C7})$$

Appendix D: Time of the maximum of roughness

In order to investigate the peak of roughness, we start with (B1), where equilibrium fluctuations are neglected:

$$\partial_{\bar{h}^{(0)}} \langle |\Sigma h_q^{(1)}(t)|^2 \rangle = -2 \frac{\lambda_{\Sigma q}}{\Omega F \bar{h}^{(0)}} \langle |\Sigma h_q^{(1)}(t)|^2 \rangle - 2\Omega L. \quad (\text{D1})$$

In the limit of slow attachment-detachment kinetics $\nu\bar{h}^{(0)}/D \ll 1$ and for $k \gg 1$, we obtain

$$\langle |\Sigma h_q^{(1)}(t)|^2 \rangle = \frac{2\Omega L}{1 - X_q} \left[\left(\frac{\bar{h}^{(0)}(t)}{\bar{h}_0^{(0)}} \right)^{X_q} - \left(\frac{\bar{h}^{(0)}(t)}{\bar{h}_0^{(0)}} \right) \right], \quad (\text{D2})$$

where

$$X_q = \frac{2\nu\Gamma c_{\text{eq}}^0}{F} q^2. \quad (\text{D3})$$

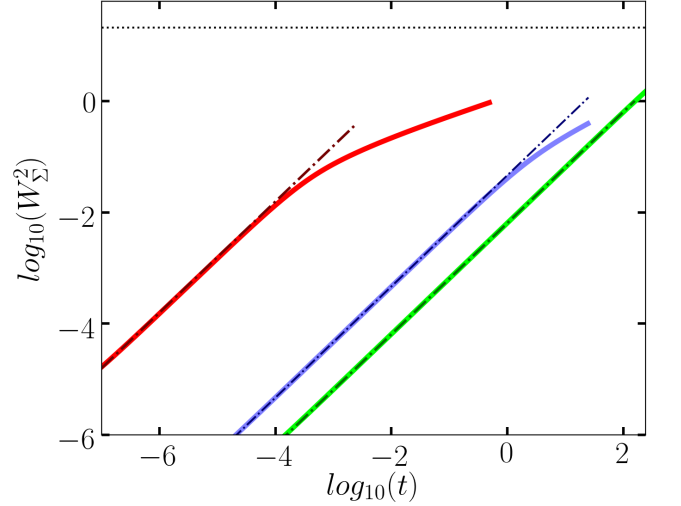


FIG. 15. Roughness at short times for different kinetics. Red $\nu = 10^{-3}$, blue $\nu = 1$, green $\nu = 10^5$. The dash-dotted lines are the solution of (C7). We have used the following model parameters: $\Omega = 1$, $D = 10^4/4$, $c_{\text{eq}}^0 = 10^{-2}$, $\Gamma = 4.05$, $L = 512$, $\bar{h}^{(0)}(0) = 32$, $F = 10^{-4}$.

For a given mode q , the roughness will reach a maximum when $\partial_{\bar{h}^{(0)}} \langle |\Sigma h_q^{(1)}(t)|^2 \rangle = 0$, i.e. when

$$t = t_{\text{peak}}^q = \frac{-\ln X_q}{\Omega F (1 - X_q)}. \quad (\text{D4})$$

Assuming that the peak is dominated by short-wavelength modes, we simply consider this condition at the microscopic cutoff $q_c = \pi/a$, leading to

$$X = X_{q_c} = \frac{2\nu\Gamma c_{\text{eq}}^0 \pi^2}{\Omega F}. \quad (\text{D5})$$

We therefore obtain an estimate of the time of the peak as

$$t_{\text{peak}} = \frac{-\ln X}{(1 - X) \Omega F}. \quad (\text{D6})$$

Appendix E: Effective exponents from the Langevin model

Fig. 16 illustrates the procedure to extract the effective exponent from the numerical solution of the Langevin model. These exponents were used to determine the position of the red and orange symbols in Fig. 8.

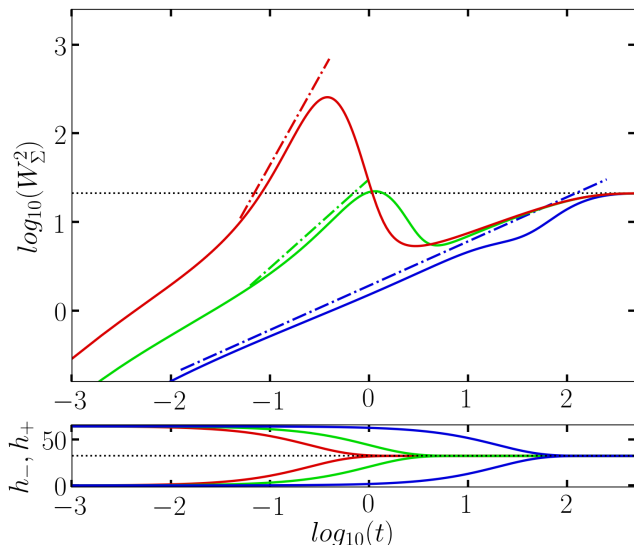


FIG. 16. Roughness of the in-phase mode for different values of F . Blue: $F = 5.10^{-2}$, green: $F = 1$, and red: $F = 4$. Dashed-dotted lines correspond to power-law scaling. Blue: $W_{\Sigma}^2 \propto t^{1/2}$, green: $W_{\Sigma}^2 \propto t$, and red: $W_{\Sigma}^2 \propto t^2$. We have used the following model parameters: $\Omega = 1$, $D = 10^4/4$, $c_{\text{eq}}^0 = 10^{-2}$, $\Gamma = 4.05$, $L = 512$, $\bar{h}^{(0)}(0) = 32$, $\nu = 10^3$.

-
- [1] P. L. Krapivsky, S. Redner, and E. Ben-Naim, *A Kinetic View of Statistical Physics* (Cambridge University Press, 2010).
- [2] R. Livi and P. Politi, *Nonequilibrium Statistical Physics: A Modern Perspective* (Cambridge University Press, 2017).
- [3] Y. Saito and H. Müller-Krumbhaar, Critical phenomena in morphology transitions of growth models with competition, *Phys. Rev. Lett.* **74**, 4325 (1995).
- [4] B. Derrida and R. Dickman, On the interface between two growing eden clusters, *Journal of Physics A: Mathematical and General* **24**, L191 (1991).
- [5] F. D. A. A. Reis and O. Pierre-Louis, Interface collisions, *Physical Review E* **97**, 040801 (2018).
- [6] Y. Saito, *Statistical Physics of Crystal Growth* (World Scientific, Singapore, 1996).
- [7] J. S. Langer, Instabilities and pattern formation in crystal growth, *Rev. Mod. Phys.* **52**, 1 (1980).
- [8] A. Be'er, H. P. Zhang, E.-L. Florin, S. M. Payne, E. Ben-Jacob, and H. L. Swinney, Deadly competition between sibling bacterial colonies, *Proceedings of the National Academy of Sciences* **106**, 428 (2009), <http://www.pnas.org/content/106/2/428.full.pdf>.
- [9] O. V. Yazyev and S. G. Louie, Electronic transport in polycrystalline graphene, *Nature materials* **9**, 806 (2010).
- [10] W. J. Evans, L. Hu, and P. Koblinski, Thermal conductivity of graphene ribbons from equilibrium molecular dynamics: Effect of ribbon width, edge roughness, and hydrogen termination, *Applied Physics Letters* **96**, 10.1063/1.3435465 (2010).
- [11] S. Merabia and K. Termentzidis, Thermal boundary conductance across rough interfaces probed by molecular dynamics, *Physical Review B - Condensed Matter and Materials Physics* **89**, 10.1103/PhysRevB.89.054309 (2014), arXiv:1501.00934.
- [12] R. Grantab, V. B. Shenoy, and R. S. Ruoff, Anomalous strength characteristics of tilt grain boundaries in graphene, *Science* **330**, 946 (2010).
- [13] Y. Ogawa, B. Hu, C. M. Orofeo, M. Tsuji, K.-i. Ikeda, S. Mizuno, H. Hibino, and H. Ago, Domain structure and boundary in single-layer graphene grown on cu (111) and cu (100) films, *The Journal of Physical Chemistry Letters* **3**, 219 (2012).
- [14] Q. Yu, L. A. Jauregui, W. Wu, R. Colby, J. Tian, Z. Su, H. Cao, Z. Liu, D. Pandey, D. Wei, T. F. Chung, P. Peng, N. P. Guisinger, E. A. Stach, J. Bao, S. S. Pei, and Y. P. Chen, Control and characterization of individual grains and grain boundaries in graphene grown by chemical vapour deposition, *Nature Materials* **10**, 443 (2011), 1011.4690.
- [15] I. Elkinani and J. Villain, Growth roughness and instabilities due to the schwoebel effect : a one-dimensional model, *J. Phys. I France* **4**, 949 (1994).
- [16] C. Misbah, O. Pierre-Louis, and Y. Saito, Crystal surfaces in and out of equilibrium: A modern view, *Rev. Mod. Phys.* **82**, 981 (2010).
- [17] W. W. Mullins and R. F. Sekerka, Morphological stability of a particle growing by diffusion or heat flow, *Journal of Applied Physics* **34**, 323 (1963), <https://doi.org/10.1063/1.1702607>.
- [18] G. S. Bales and A. Zangwill, Morphological instability of a terrace edge during step-flow growth, *Phys. Rev. B* **41**,

- 5500 (1990).
- [19] F. D. A. A. Reis, B. Marguet, and O. Pierre-Louis, Growth at high substrate coverage can decrease the grain boundary roughness of 2d materials, arXiv:2204.01894 (2022).
- [20] R. L. Schwoebel and E. J. Shipsey, Step motion on crystal surfaces, *Journal of Applied Physics* **37**, 3682 (1966).
- [21] R. L. Schwoebel, Step motion on crystal surfaces. ii, *Journal of Applied Physics* **40**, 614 (1969).
- [22] T. Michely and J. Krug, *Islands, Mounds, and Atoms* (Springer, 2003).
- [23] O. Pierre-Louis and C. Misbah, Dynamics and fluctuations during mbe on vicinal surfaces. i. formalism and results of linear theory, *Phys. Rev. B* **58**, 2259 (1998).
- [24] A.-L. Barabasi and H. Stanley, *Fractal Concepts in Surface Growth* (Cambridge University Press, Cambridge, England, 1995).
- [25] Y. Saito, M. Dufay, and O. Pierre-Louis, Nonequilibrium cluster diffusion during growth and evaporation in two dimensions, *Phys. Rev. Lett.* **108**, 245504 (2012).
- [26] L. Gagliardi and O. Pierre-Louis, Controlling anisotropy in 2d microscopic models of growth, *Journal of Computational Physics* **452**, 110936 (2022).
- [27] R. E. Caflisch, W. E. M. F. Gyure, B. Merriman, and C. Ratsch, Kinetic model for a step edge in epitaxial growth, *Phys. Rev. E* **59**, 6879 (1999).
- [28] P. Politi and J. Villain, Ehrlich-schwoebel instability in molecular-beam epitaxy: A minimal model, *Phys. Rev. B* **54**, 5114 (1996).